LOAN DOCUMENT

PHOTOGRAPH THIS SHEET

DTIC ACCESSION NUMBER

LEVEL

INVENTORY

CU-1091/8

DOCUMENT IDENTIFICATION

1 Dec 98

DISTRIBUTION STATEMENT A
Approved for Public Release
Distribution Unlimited

DISTRIBUTION STATEMENT

ACCESSION FOR

NTIS	GRA&I	☑
DTIC	TRAC	☐
UNANNOUNCED		☐
JUSTIFICATION		

BY

DISTRIBUTION/

AVAILABILITY CODES

DISTRIBUTION	AVAILABILITY AND/OR SPECIAL

A-1

DISTRIBUTION STAMP

DATE ACCESSIONED

DATE RETURNED

H
A
N
D
L
E

W
I
T
H

C
A
R
E

DTIC QUALITY INSPECTED 4

20000720 095

DATE RECEIVED IN DTIC

REGISTERED OR CERTIFIED NUMBER

PHOTOGRAPH THIS SHEET AND RETURN TO DTIC-FDAC

DTIC FORM 70A
JUN 90

DOCUMENT PROCESSING SHEET

PREVIOUS EDITIONS MAY BE USED UNTIL
STOCK IS EXHAUSTED.

LOAN DOCUMENT

INNOVATIVE SEISMIC SYSTEM FOR BURIED UNEXPLODED ORDNANCE DETECTION AND CLASSIFICATION

CU-1091/8

December 1, 1998

Performing Organization:

GTE – BBN Technologies
70 Fawcett Street
Cambridge, MA 02138
Phone 617 873-4158
Fax 617 873-2918
email pak@bbn.com

PRINCIPAL INVESTIGATORS: Peter A. Krumhansl, Carey Bunks, Jay Pulli

Submitted to:

Executive Director
SERDP Program Office
901 North Stuart Street, Suite 303
Arlington, VA 22203-1821

REPORT DOCUMENTATION PAGE

Public reporting burden for this collection of information is estimated to average 1 hour per response, including the time for reviewing instructions, searching existing data sources, gathering and maintaining the data needed, and completing and reviewing this collection of information. Send comments regarding this burden estimate or any other aspect of this collection of information, including suggestions for reducing this burden to Washington Headquarters Services, Directorate for Information Operations and Reports, 1215 Jefferson Davis Highway, Suite 1204, Arlington, VA 22202-4302, and to the Office of Management and Budget, Paperwork Reduction Project (0704-0188), Washington, DC 20503

1. AGENCY USE ONLY (Leave blank)	2. REPORT DATE December 1, 1998	3. REPORT TYPE AND DATES COVERED Annual Report FY 1998

4. TITLE AND SUBTITLE
Innovative Seismic System for Buried Unexploded Ordnance Detection and Classification

5. FUNDING NUMBERS
N/A

6. AUTHOR(S)
Krumhansl, Peter A., Carey Bunks, and Jay Pulli

7. PERFORMING ORGANIZATION NAME(S) AND ADDRESS(ES)

GTE-BBN Technologies
70 Fawcett Street
Cambridge, MA 02138

8. PERFORMING ORGANIZATION REPORT NUMBER
N/A

9. SPONSORING / MONITORING AGENCY NAME(S) AND ADDRESS(ES)
SERDP
901 North Stuart St. Suite 303
Arlington, VA 22203

10. SPONSORING / MONITORING AGENCY REPORT NUMBER
N/A

11. SUPPLEMENTARY NOTES

12a. DISTRIBUTION / AVAILABILITY STATEMENT	12b. DISTRIBUTION CODE
Approved for public release: distribution is unlimited.	A

13. ABSTRACT *(Maximum 200 Words)*

Unexploded ordnance (UXO) presents a lethal hazard to individuals worldwide in previous war zones and at military training facilities. At Department of Defense installations in this country, it is estimated that over 10,000 sites and 11,000,000 acres are contaminated with hazardous materials. Many areas are now scheduled to be returned to civilian use or require environmental cleanup, which necessitates a thorough and efficient site characterization and remediation process.

Current UXO sensing technologies, including magnetometers and EM sensors, have been used for a long time for reconnaissance mapping and are becoming highly efficient for mapping large areas. These sensors detect the ferrous metal content or electrical conductivity properties of buried materials. Detection rates for these sensors can be as high as 95%, depending on the soil and UXO characteristics.

14. SUBJECT TERMS
SERDP, SERDP Collection, unexploded ordnance, UXO, seismic system

15. NUMBER OF PAGES
91

16. PRICE CODE
N/A

17. SECURITY CLASSIFICATION OF REPORT	18. SECURITY CLASSIFICATION OF THIS PAGE	19. SECURITY CLASSIFICATION OF ABSTRACT	20. LIMITATION OF ABSTRACT
unclass	unclass	unclass	UL

NSN 7540-01-280-5500

Standard Form 298 (Rev. 2-89)
Prescribed by ANSI Std. Z39-18
298-102

Table of Contents

INNOVATIVE SEISMIC SYSTEM FOR BURIED UNEXPLODED ORDNANCE DETECTION AND CLASSIFICATION

CU-1091/8

Performing Organization

GTE - BBN Technologies

PRINCIPAL INVESTIGATORS: Peter A. Krumhansl, Carey Bunks, Jay Pulli
GTE – BBN Technologies, 70 Fawcett Street, Cambridge, MA 02138
Phone 617 873-4158
Fax 617 873-2918
email pak@bbn.com

1. Introduction

1.1 Project Background

Unexploded ordnance (UXO) presents a lethal hazard to individuals worldwide in previous war zones and at military training facilities. At Department of Defense installations in this country, it is estimated that over 10,000 sites and 11,000,000 acres are contaminated with hazardous materials. Many areas are now scheduled to be returned to civilian use or require environmental cleanup, which necessitates a thorough and efficient site characterization and remediation process.

Current UXO sensing technologies, including magnetometers and EM sensors, have been used for a long time for reconnaissance mapping and are becoming highly efficient for mapping large areas. These sensors detect the ferrous metal content or electrical conductivity properties of buried materials. Detection rates for these sensors can be as high as 95%, depending on the soil and UXO characteristics. Unfortunately, these systems detect a lot of inert metal objects in

the ground or naturally occurring materials that cannot be differentiated from UXO. The false target rate can run as high as 10:1 or higher. The unnecessary excavation of this clutter, especially for deeper buried objects, greatly inflates the cost of the cleanup process.

Refinements in processing and inversion are improving the magnetometer and EM sensor capabilities, but discrimination of ordnance from a similar size piece of steel fragment has remained difficult. Multi-sensor fusion of the two sensors has limited potential because the magnetic response and conductivity properties are both dependent on the quantity of steel, which may be similar for ordnance and non-ordnance objects. The two sensors don't provide sufficiently independent information to discriminate between non-ordnance ferrous objects and live ordnance.

Seismic technologies have proven highly successful in oil exploration, geotechnical, and environmental work. A seismic system interrogates the *mechanical properties of buried objects*: their mechanical stiffness, size, shape, total mass, and overall structural response to vibration. An intact bomb with several hundred pounds of explosive has a different total mass and mechanical response to vibration than a crumpled fragment of steel. A seismic system, which generates vibrational waves that sample an object's response, can discriminate between the two. Used in a sensor fusion process, the seismic response provides a truly independent measure of the properties of buried objects.

Environmental factors play a dominant role in the effectiveness of all UXO sensor technologies. In some soils, which have high magnetic mineral content or are highly conductive due to clay or ion content, current sensors become ineffective. Development of a seismic ordnance detection system will provide an additional tool to overcome environmental limitations.

Though continued development of the current sensing technologies may yield incremental improvements, developing a new sensor that detects different properties of the buried ordnance and can operate in areas that are difficult for the other sensors would greatly improve the efficiency of detection and classification of UXO. Significant savings will be achieved for DOD site remediation by incorporation of a seismic sensor into an appropriately structured site characterization and cleanup process.

1.2 Objective

The objective of this research effort is to develop a new seismic ordnance detection system (SODS) adapted specifically to the detection and discrimination of UXO from other clutter. Current seismic technologies for larger scale problems are not directly applicable, but do provide a technology base from which to draw. The seismic ordnance detection system must be based on higher frequencies than other methods and we are performing a system analysis to investigate the potential capabilities and performance at these frequencies. This analysis, along with development and testing of a proof-of-concept system consisting of hardware and software, constitutes a three-year program.

The technical objectives to be accomplished over three years are:

- Year 1—Perform an initial feasibility study to analyze practicality of seismic UXO detection using short wavelength seismic waves. A system simulation/analysis will be developed incorporating field measurement of seismic sources, receivers, wave propagation, and noise. Propagation and UXO seismic response will be modeled to analyze detection performance and clutter. This system simulation tool will be used to design a proof-of-concept system.

- Year 2—Develop a proof-of-concept SODS system for testing. We will develop seismic sources and receivers and engineer a practical, mobile array of seismic transducers that can be used to efficiently collect data to investigate buried UXO. We will study implementations of the receiver/source array/beamformer to improve the target signal-to-noise ratio and minimize clutter. Initial testing will evaluate components and system performance. Later testing with buried UXO objects will be used to assess and refine components and methods. Analysis of the resulting seismic data will focus on deriving information useful for discrimination in a multi-sensor process.

- Year 3—Evaluate SODS in controlled testing. This effort will include refinement of the proof-of-concept system and analysis of detections of UXO to evaluate target/clutter discrimination capabilities. This will culminate in an initial evaluation of SODS in multisensor tests and an analysis of false

alarm reduction using seismic data in sensor fusion processes. After completing tests of the proof-of-concept system, a new specification will be developed for a fieldable system that could be more rigorously field-tested in the future, possibly in the ESTCP program.

This annual report covers the first year's efforts. Some analysis tasks are not completed and funding is not fully expended, due to the late start of the funding.

During this first year there have been a number of contributors to the research and to this report in addition to Peter Krumhansl. Robert Barile, Eugene Dorfman, and Henno Allik have performed the target response modeling work. Carey Bunks and Mike Goldsmith have performed signal processing, field data collection, and simulation tasks. Chris Remer and Jay Pulli have assisted with data acquisition, analysis tasks, and development of the web site.

1.3 First Year Technical Approach Overview

The feasibility study of this year has focused on two basic questions: (1) investigating the detectability of UXO with seismic waves and (2) developing an understanding of the features of the seismic response that can be used to distinguish UXO from clutter. These questions have been addressed with a system concept in mind, though other approaches to the problem will be considered in light of the analysis.

1.3.1 Seismic Sonar Concept

A seismic system for the detection and classification of UXO in soil has similarities to both a reflection seismic imaging system and an active sonar system. In previous research work under contract to the US Army, BBN developed a seismic sonar system concept and successfully applied it to detecting very shallow buried antitank mines.

Through conversations with operators and researchers of current sensors it is clear that high rates of reconnaissance mapping can be accomplished with magnetometers and EM sensing technologies. Though the seismic technology is also capable of mapping of areas at reasonable efficiency, we are focusing on a

system concept which will provide the maximum amount of information about the seismic response of a target at an approximately known location.

The target oriented seismic sonar system concept is illustrated in Figure 1-1.
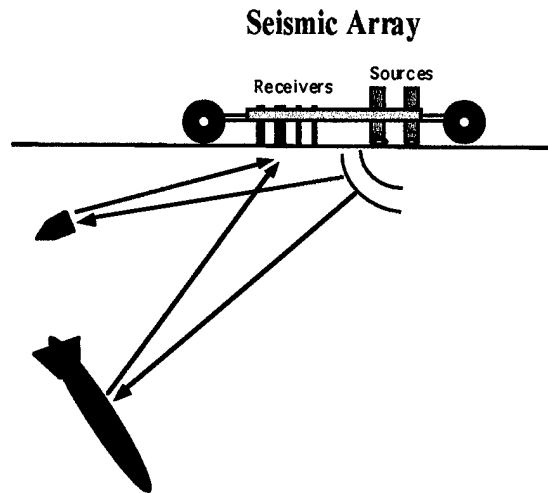
Seismic Array

Figure 1-1. Target Oriented Seismic Sonar System Concept

Once an area has been determined to contain one or more potential ordnance objects, an array of seismic sources and receivers is placed on the surface in the vicinity of the area to be investigated. The seismic sources generate vibrations, which propagate through the ground as waves. When they encounter an object with different mechanical properties than the surrounding soil, the object moves, rotates, and resonates, resulting in scattered waves. These scattered waves are sensed by receivers on the surface, and their output is individually recorded digitally. A computer then beamforms or images the data by scanning or focusing the array at each point in the search area. If scattered energy is coming from an object, it produces a signal at that location in the beamformed image, which is displayed for the operator. The detected signal can be further analyzed to classify the target.

1.3.2 Seismic Waves for Subsurface Detection

The difference between an acoustic sonar system and a seismic system is that there are different waves propagating in the ground in addition to the compressional wave in acoustics. A seismic source that applies a vertical point force on the surface of the soil produces a variety of propagating seismic wave

types. Unlike acoustic media, which cannot transmit shear stress, an elastic medium such as soil propagates both compressional P waves and shear S waves. These waves travel through the volume of the subsurface and have particle motion that is polarized longitudinally and transverse to the direction of propagation, respectively (Figure 1-2). Additionally, from a surface seismic source, Rayleigh waves propagate along the boundary with an elliptical particle motion polarization. The particle motion of Rayleigh waves dies off rapidly with depth, extending down only about a wavelength. Any of these wave types can be used as the basis for a subsurface detection system, depending on the goal of the survey, but for objects buried below the surface, the compressional and shear waves are the best candidates. Earlier investigations indicated that shear waves would be the best candidate for UXO detection because of their lower speed, shorter wavelength, later arrival in the reverberation decay. Therefore, system analysis for SODS is focussing initially on shear waves.
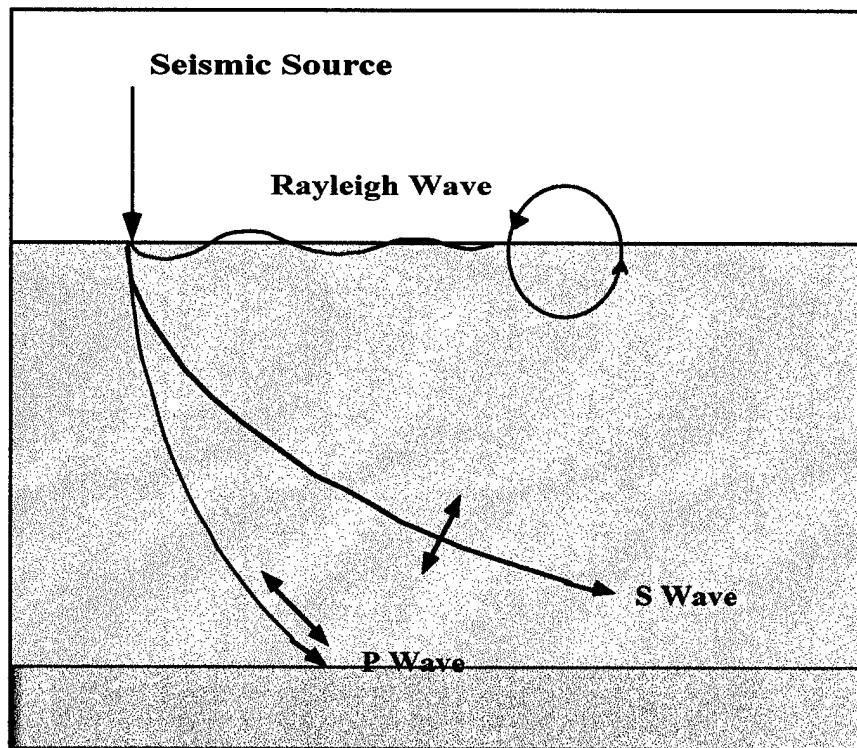
Figure 1-2. Seismic wave types from a vertical surface point source.

1.3.3 Analysis Approach

In the feasibility study, we have approached the analysis of the detectability of the seismic response of UXO in the presence of noise by using the general framework of the sonar equation. This approach breaks the problem into measurable quantities, as illustrated in Figure 1-3.
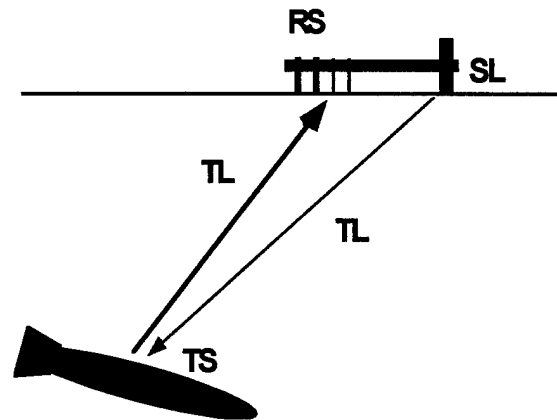
$$SNR = SL - TL + TS - TL + RS + AG + PG - N - REV$$

SL = Source Level   PG= Processing Gain

TL = Transmission Loss   N = Ambient and Sensor Noise

TS = Target Strength   REV = Reverberation

RS = Receiver Sensitivity

AG = Array Gain

Figure 1-3. The Sonar Equation

The seismic wave is generated by the source producing a small measurable ground velocity or acceleration at a reference distance, which is termed source level (SL). The wave travels through the ground and the level is reduced due to geometric spreading and absorption, called the transmission loss (TL). At the target, a portion of the energy incident is scattered; this is the target strength (TS). The scattered energy, which is the signal we want to detect, travels back to the receiver and is reduced again by transmission loss (TL) . The receiver senses

this signal, but it also senses ambient noise (N) and reverberation (REV). The receiver turns the ground vibration into voltage proportional to the receiver sensitivity (RS). This voltage is added to the electronic noise of the sensor and recording system. Once recorded, the signals from many receivers can be processed together to enhance the signal and reduce all forms of noise (AG). If all the terms are expressed in dB, they can be added, as in the above equation, to get signal-to-noise ratio of the target response.

In a seismic system, many of the quantities described above are more complicated than single numbers and are functions of wave type, frequency, and angle of propagation in the ground.

In this first year, we are obtaining quantitative information for each of the terms in the equation, either by making field measurements in natural soils or by analysis and modeling. These multidimensional quantities are combined in a system simulation, which allows analysis of the impact of the components on the detection signal-to-noise ratio. We then use this simulation/testbed for array design, beamformer development and testing, and performance prediction.

The research program is composed of three technical tasks, which will be discussed in detail in the following sections: Target Response Modeling, Seismic Field Tests, and System Simulation.

2. Target Response Modeling

2.1. Introduction

2.1.1. Objectives

The target response modeling task has focused on answering two questions for determination of the feasibility of seismic ordnance detection:

1. How much seismic energy is reflected from a buried ordnance object? What is its effective target strength, and what is the frequency dependence?

2. What distinctive characteristics of the seismic target response can be used to distinguish intact live ordnance from fragments?

2.1.2. Approach

We have approached these questions with two different modeling approaches: analytic elastic modeling and finite element modeling (FEM). There are analytical solutions for elastic wave scattering from simple shaped elastic objects in elastic media. These solutions are for solid objects of simple shape. The analytic models can provide simple target strength values for system design, but addressing the second question about distinctive features of the seismic response is key to determining the value of SODS. Answering the second question requires a more realistic, detailed representation of the object with different materials and complex shape. This is better done with a finite element model, which can accurately represent the main structural features of a piece of ordnance. Finite difference approaches are not a good alternative for addressing the second question, because they require a relatively coarse approximation to the actual object and would be impractical for a 3D object.

In order to perform finite element modeling for UXO in soil we needed to extend the capabilities of the SARA FEM code used for submarine target strength analysis. This code allows modeling of axisymmetric objects embedded in infinite

acoustic media. For the UXO problem we added capabilities to include elastic infinite media and added of incident and scattered shear waves.

The following three sections present our work to date in analytic modeling of a steel sphere, SARA FEM Code Development, and FEM Modeling results of a 15″ steel sphere and a 155mm shell. The steel sphere was used for comparing results of both analytic methods and Finite Element Methods. The 155mm shell was chosen because it is intermediate in size and weight in the range of ordnance between mortar shells and bombs. We were also able to obtain an inert 155mm shell for tests.

2.2. Analytical Solution

2.2.1. Background

The analytical solution for shear (i.e., transverse elastic) plane wave scattering from an elastic sphere immersed into the elastic medium was first presented in Reference [2-1]. Derivation is straightforward but tedious. The solution involves solving linear system of four complex equations. Subsequent to this paper, in Refs. [2-2, 2-3], several errors in the derivation [2-1] were corrected, and the Born approximation for the scattered field was developed, which is valid for small contrast objects.

For the UXO modeling effort, the exact solution [2-1] with corrections [2-2, 2-3] was reformulated in terms of tabulated special functions and implemented in Matlab. The linear system of four complex equations was inverted numerically. Solution was found stable for $ka < 16\pi$, where a is the sphere radius, and k is the incident wavenumber.

2.2.2. Benchmarking Effort

Our analytic solution for a small low contrast sphere was compared to the Born approximation solution [2-4]. For the parameters used, the Born approximation can be used as a benchmark. We found that our solution matches [2-4] except for a "reversed" forward and back directions: backscattering direction in [2-4] corresponds to forward scattering direction in our solution, and vice versa. To identify true forward direction, we solved for the scattering from a large, stiff, heavy

object. Since we expect to see a shadow behind such an object, the scattered field must have a strong lobe into the forward direction ("shadow forming lobe"). Our solution, indeed, demonstrated a strong lobe approaching forward direction as object size increases, while solution [2-4] placed this lobe in the backscattering direction. Although these benchmarks did not deliver a positive proof that our solution is correct, and more work may be needed to guarantee correctness, we achieved some level of confidence in our solution.

2.2.3. In Plane Scattering: Steel Sphere Target Strength

For the UXO systems analysis effort, the target strength was computed for a 15-inch steel sphere buried in the soil due an incident shear wave. Target strength values were obtained separately for the resulting scattered shear and compressional waves (Figs. 2-1 and 2-2, respectively), as a function of frequency and scattering angle in the plane of scattering. The values are farfield values normalized to a reference distance of 1 meter. It is seen in the figures below, for the case considered, most of the incident elastic energy is scattered into the shear wave with a average target strength of –17 dB over the seismic band from 100 to 1600 Hz.
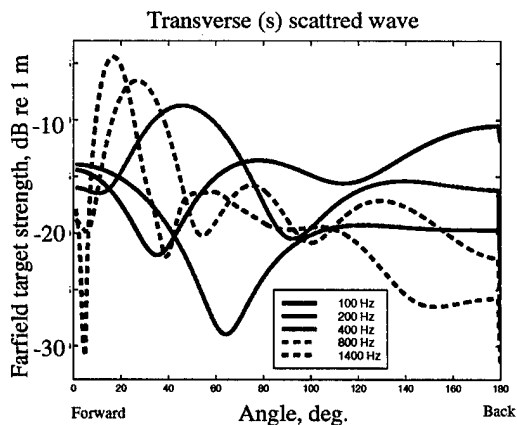

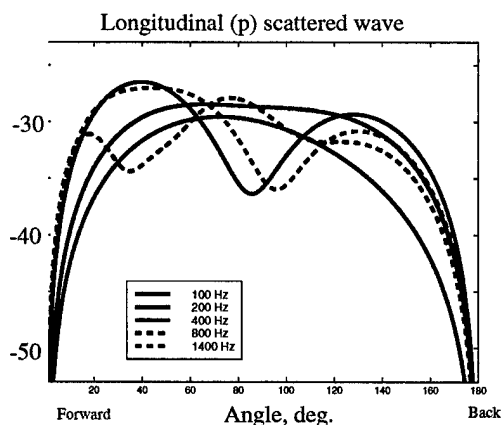Figure 2-1. Transverse wave scattered from a steel sphere buried in the soil.

Figure 2-2. Longitudinal wave scattered from a steel sphere buried in the soil.

2.3. SARA Finite Element Code Development

2.3.1. Introduction

The response of a structure surrounded by an infinite elastic medium is usually treated by dividing the problem space into a near-field region and a far-field region. The near-field region contains the inhomogeneities and the geometric complexities, which are readily modeled by standard finite element methods. The far field is usually treated as an isotropic elastic solid which needs to be truncated at some distance and supplied with a nonreflecting boundary condition. A cost-effective method for treating the truncated boundary is the infinite element [2-5]. Cost-effectiveness of the infinite element method derives from the following two sources: use of the method leads to a banded set of equations that can be solved efficiently, and it permits the use of a smaller near-field model than other methods.

The SARA-2D [2-6] code uses the finite element, infinite element technique to solve radiation and scattering problems. Although the infinite medium is an acoustic fluid, SARA nevertheless contains many of the capabilities needed for UXO modeling. Specifically, the embedded object and the surrounding elastic near field can be modeled with existing finite elements. The application of boundary constraints and the representation of forcing functions are also in place. In order to model the UXO problem new development was needed in three areas:

a) Elastodynamic infinite element

b) Elastodynamic plane wave loadings

c) Elastodynamic field equations

2.3.2. Elastodynamic Infinite Element

Various successful infinite elements have been derived and used for scalar wave problems. In elasticity problems the situation is more complicated due to the existence of multiple wave types. Two types of body waves can be sustained: dilatation or P-waves, and shear waves consisting of SV (vertical) and SH (horizontal). When a free surface is present a Rayleigh wave also is present. Including multiple wave types in an infinite element has been accomplished in [2-7], but the resulting element violates finite element consistency and compatibility requirements. It is also expensive to compute, requiring many integration points in the infinite direction. Several researchers have extended the development, e.g., [2-8], but all are elaborate, expensive developments. There are examples [2-9] that a simpler, single wave type of elastic element might suffice for our problem. This approach would make approximations as to the wavenumber to be used in a given problem. Generally the wavenumber of the dominant field is used, which in the UXO case is probably shear.

We have recently implemented a wave envelope [2-10] type of infinite element in SARA for structural acoustics problems. The main attractiveness of the element is that the matrices are not frequency dependent and hence need be computed only once during a run. The frequency independence also means that no special integration rules are necessary and standard Gaussian quadrature can be used. Our implementation used high-order polynomials in the infinite direction (the p-method) in order to further reduce the extent of the near-field model. An elastodynamic version of the wave envelope element was developed for modeling the UXO problem in SARA.

2.3.2.1. *Governing Equations*

The elastodynamics equilibrium equations in discretized form under harmonic loadings can be written as

$$\left(K - \omega^2 M\right)U = F \qquad (2\text{-}1)$$

13

where K and M are the global stiffness and mass matrices, $U = <u\ v\ w>$ is the vector of displacements, F is the vector of applied loads and ω is the circular excitation frequency. The global matrices are assembled from element matrices

$$K = \iiint B^T D\ B\ dV \qquad (2\text{-}2)$$

$$M = \iiint N^T \rho N\ dV \qquad (2\text{-}3)$$

$$F = \iint N^T T\ dA + N^T\ P \qquad (2\text{-}4)$$

where N is the matrix of shape functions for the element, B is the strain-displacement matrix, D contains the constitutive constants which can in general be complex and frequency dependent, T is the traction vector and P represents concentrated loads. The integrals are over the volume V and area A of the element. In our axisymmetric problem everything is expressed in cylindrical coordinates and displacements and forces are expressed in a Fourier series in terms of the circumferential coordinate. Thus equations (2-1 through 2-4) are used to solve the problem for one Fourier harmonic n and the total solution is obtained by superposition of harmonics evaluated at any circumferential position. The matrix B, and hence also K, is a function of n and the forces F can be as well.

To arrive at equations (2-1 through 2-4) the displacements are first expressed in terms of polynomial shape functions N and unknown nodal displacements as

$$U = \sum_i N_i U_i\ . \qquad (2\text{-}5)$$

The finite element representation then follows through the application of standard procedures [2-11] such as minimization of energy or Galerkin's method of weighted residuals. In the method of weighted residuals the weighting function is taken equal to the shape function and hence the resulting stiffness and mass matrices are nicely symmetric. The embedded structure and the near field of the surrounding medium can be modeled with such finite elements. The unbounded

far-field region of the outer medium, however, requires a special shape functions that describes the behavior of the solution with increasing distance from the embedded structure. The displacements are now expressed as

$$U = \sum \phi_j U_j = \sum N_j \ exp(-ik\mu) U_j \qquad (2\text{-}6)$$

where N is an interpolation function expressed in powers of reciprocal radial coordinate and μ is a radial distance (see the next section for specifics). At the finite element infinite element interface the phase in Eq. (2-6) is set to one $(\mu=0)$ for compatibility with the near field region.

The approximation that is made at this stage is to use a wavenumber k to describe the outgoing wave when in reality we know that multiple wave types are present. In applications the wavenumber can be set to that of the expected dominant wave in the problem and can be changed in various regions of the model.

In contrast to the finite element formulation the weighting function in the wave envelope elements is not taken to be the same as the shape function. Instead the weighting function W is specified as

$$W = D \bullet N \ exp \ (+ik\mu) \qquad (2\text{-}7)$$

where D is a factor proportional to the inverse square of the radius and is unity at the inner edge of the element. D is needed in order to make some of the integrals finite (see [2-10] for details). When equations (2-6) and (2-7) are used in the weighted residuals procedure then the expressions equivalent to equations (2-2) and (2-3) are

$$K = \iiint B^T(W) \ D \ B(\phi) \ dV \qquad (2\text{-}8)$$

and

$$M = \iiint W^T \rho\,\phi\,dV \qquad\qquad (2\text{-}9)$$

where B is now considered to be the strain-displacement operator given by

$$B^T = \begin{bmatrix} \dfrac{\partial}{\partial r} & \dfrac{1}{r} & 0 & \dfrac{\partial}{\partial z} & -\dfrac{n}{r} & 0 \\[2ex] 0 & \dfrac{n}{r} & 0 & 0 & \dfrac{\partial}{\partial r}-\dfrac{1}{r} & \dfrac{\partial}{\partial z} \\[2ex] 0 & 0 & \dfrac{\partial}{\partial z} & \dfrac{\partial}{\partial r} & 0 & -\dfrac{n}{r} \end{bmatrix} \qquad (2\text{-}10)$$

Note that the exponential term in the weighting function is the complex conjugate of the exponential in the shape function and hence cancels in the products of Eqs. (2-8) and (2-9). This allows standard Gauss quadrature to be used for integration and results in element matrices independent of frequency. After performing the products the resulting element equations can be written by powers of ω as

$$\left[K + i\omega\,C + (i\omega)^2 M\right] U = F \qquad\qquad (2\text{-}11)$$

All of the terms in C are derived from Eq. (2-8) and M contains terms from both Eqs. (2-8) and (2-9). The forces F are the same as in Eq. (2-4) because they are likely to be applied only at the inner surface of the wave envelope element where W and ϕ are equal.

2.3.2.2. Geometry and Shape functions

The nodal numbering and the natural coordinate system for the wave envelope element are shown in Figure 2-3. A two-dimensional, mapped, Lagrange infinite element is shown in the figure along with the mapping functions. The derivatives may be found in reference [2-5], although the nodal order is different. Note that $\xi=-1$ is at the near-field far-field interface and $\xi=1$ is at infinity. The nodes at $\xi=0$ define the virtual sources from where the outwardly propagating wave is

assumed to emanate (i.e., the distance from the origin to node 1 is the same as the distance from node 1 to 2). These mapping functions are used to transform local derivatives to global through the Jacobian matrix for use in Eq. (2-8). The quantity μ is given by

$$\mu = a(\eta)\frac{(1+\xi)}{(1-\xi)}$$

(2-12)

and the factor D is

$$D = \left(\frac{1-\xi}{2}\right)^2$$

(2-13)
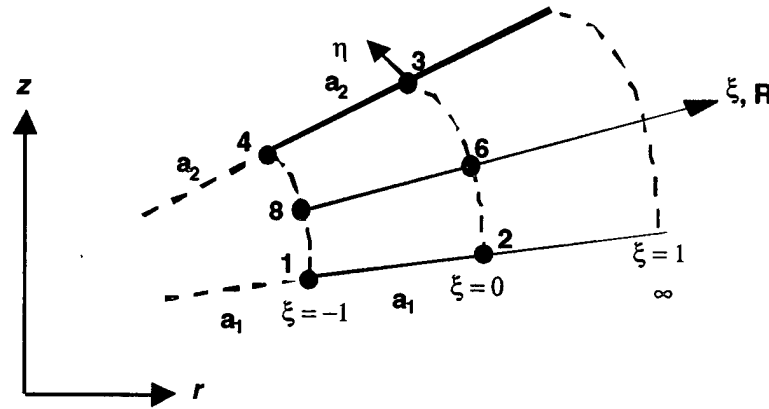
$$\xi = 1 - \frac{2a}{R} \quad or \quad R = \frac{2a}{1-\xi}$$

$$a(\eta) = \left(\frac{1-\eta}{2}\right)a_1 + \left(\frac{1+\eta}{2}\right)a_2$$

$$r = \sum M_i r_i, \quad z = \sum M_i z_i$$

where

$$M_1 = \frac{\xi\eta(1-\eta)}{(1-\xi)} \qquad\qquad M_4 = \frac{-\xi\eta(1+\eta)}{(1-\xi)}$$

$$M_2 = \frac{-\eta(1-\eta)(1+\xi)}{2(1-\xi)} \qquad\qquad M_6 = \frac{(1-\eta^2)(1+\xi)}{(1-\xi)}$$

$$M_3 = \frac{\eta(1+\eta)(1+\xi)}{2(1-\xi)} \qquad\qquad M_8 = \frac{-2\xi(1-\eta^2)}{(1-\xi)}$$

Figure 2-3. Wave-Envelope Element Geometry

The shape functions for the elastodynamic wave envelope element are developed for a variable order p-extension element starting with a "quadratic" to a ninth order element. The functions for a quadratic element are given in Figure 2-4 showing the six nodes where the displacements are defined. For the higher-order terms hierarchic polynomials with derivative degrees-of-freedom are used as shown in Figure 2-5. Each increase in the order of the polynomial adds nine degrees of freedom to the element and represents a departure from the previous order, hence p=3 is a departure from quadratic displacements, p=4 is a departure from p=3, etc. The p-method is applied only in the direction toward infinity, the tangential direction remains quadratic.

$$N_1 = \frac{\xi\eta(1-\xi)(1-\eta)}{4}$$

$$N_2 = \frac{-\eta(1-\eta)(1+\xi)(1-\xi)}{2}$$

$$N_3 = \frac{\eta(1+\eta)(1+\xi)(1-\xi)}{2}$$

$$N_4 = \frac{-\xi\eta(1-\xi)(1+\eta)}{4}$$

$$N_6 = (1-\eta^2)(1+\xi)(1-\eta)$$

$$N_8 = \frac{-\xi(1-\xi)(1-\eta^2)}{2}$$

$$N \sim \frac{a}{R} + \frac{b}{R^2}$$

□ *Geometry node*
● *Displacement node*

Figure 2-4. "Quadratic" Wave-Envelope Element

Figure 2-5. Hierarchic p-Extension Wave Envelope Element

2.3.3. Elastodynamic Plane Wave Loadings

In order to determine the loadings on the UXO structure due to incident plane waves, equations for the six stress components were derived for each of three wave types, P,SV and SH. The resulting expressions presented in Appendix A are in terms of Bessel functions for each Fourier harmonic. From these six stress components the normal and tangential tractions acting on the body at each point can be determined. The distributed load vector is then obtained for each finite element from the area integral in Eq. (2-4).

2.3.4. Elastodynamic Field Equations

If the displacement U and traction T vectors are known on the surface of a region then the displacements anywhere in the field can be determined from the elastodynamic integral equation [2-12] (see Figure 2-6 for geometry):
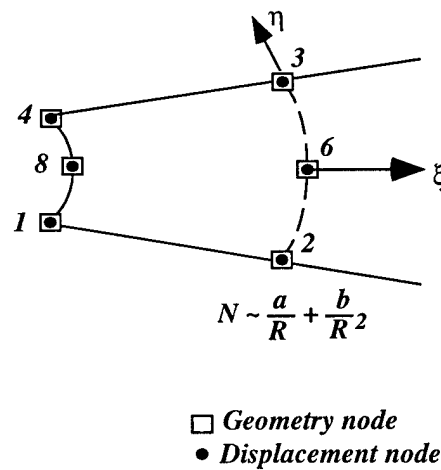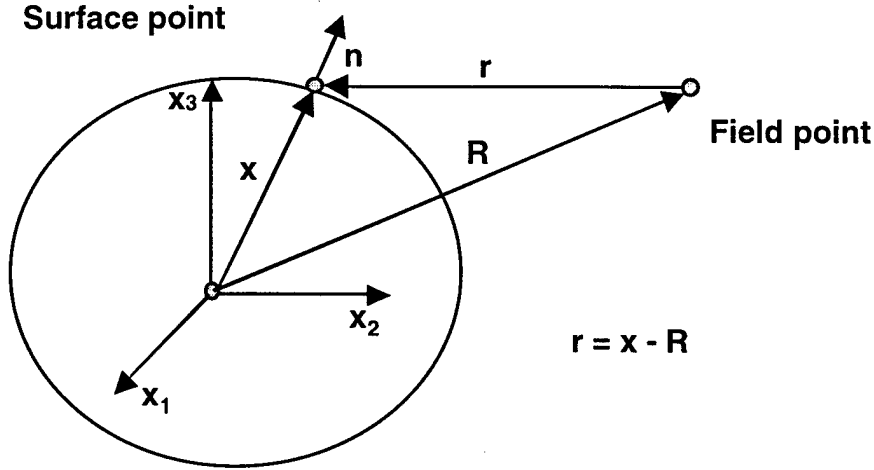
Figure 2-6. Geometry for Field Displacements

$$U_k(R,\omega) = \frac{1}{4\pi} \iint \left[T_i(x,\omega) A_{ik}(x,R,\omega) \frac{1}{\rho} - U_i(x,\omega) n_i B_{ik}(x,R,\omega) \right] ds(x) \qquad (2\text{-}14)$$

where the 3x3 matrix multiplying the tractions is given by

$$A_{jk} = \left(\frac{3 r_j r_k}{r^3} - \frac{\delta_{jk}}{r} \right) \left[\frac{1}{\omega^2 r^2} \left(exp(ik_2 r) - exp(ik_1 r) \right) \right.$$

$$\left. - \frac{i}{\omega r} \left(\frac{1}{c_2} exp(ik_2 r) - \frac{1}{c_1} exp(ik_1 r) \right) \right]$$

$$+ \frac{r_j r_k}{r^3} \left(\frac{1}{c_1^2} exp(ik_1 r) - \frac{1}{c_2^2} exp(ik_2 r) \right)$$

$$+ \frac{\delta_{jk}}{r c_2^2} exp(ik_2 r)$$

and the matrix multiplying the displacements is given by

$$B_{jk} = -6c_2^2 \left[\frac{5r_j r_k r_\ell}{r^5} - \frac{\delta_{ik} r_\ell + \delta_{k\ell} r_j + \delta_{\ell j} r_k}{r^3} \right]$$

$$\bullet \left[\frac{1}{\omega^2 r^2} \left(exp(ik_2 r) - exp(ik_1 r) \right) - \frac{i}{\omega r} \left(\frac{1}{c_2} exp(ik_2 r) - \frac{1}{c_1} exp(ikr_1) \right) \right]$$

$$+2 \left[\frac{6r_j r_k r_\ell}{r^5} - \frac{\delta_{jk} r_\ell + \delta_{k\ell} r_j + \delta_{\ell j} r_k}{r^3} \right] \bullet \left[exp(ik_2 r) - \frac{c_2^2}{c_1^2} exp(ik_1 r) \right]$$

$$- \frac{2_i i k_2 r_j r_k r_\ell}{r^4} \left[exp(ik_2 r) - \frac{c_2^3}{c_1^3} exp(ik_1 r) \right]$$

$$- \frac{r_k \delta_{i\ell}}{r^3} \left(1 - 2\frac{c_2^2}{c_1^2} \right) (1 - ik_1 r) exp(ik_1 r)$$

$$- \frac{\delta_{jk} r_\ell + \delta k_\ell r_j}{r^3} (1 - ik_2 r) exp(ik_2 r)$$

where $\delta_{jk} = \begin{cases} 1, j = k \\ 0, j \neq k \end{cases}$

$k_1 = \dfrac{\omega}{c_1}$ $c_1 = $ *speed of irrotational wave*

$k_2 = \dfrac{\omega}{c_2}$ $c_2 = $ *speed of equivoluminal wave*

2.4. FEM Modeling Results

The SARA2D (SUPER2D) code was recently updated to include elastic infinite element capability and the validation is in progress for farfield calculations but is not yet complete. We do have partial validation; the new infinite elements have been checked for P and S waves. The farfield response will be validated as time and money allow.

The SARA2D finite element analysis of a solid steel sphere and a 155-millimeter mortar shell have been done and computed results at the boundaries of the objects are presented. This memorandum discusses the geometry, loading conditions and results of the analysis.

2.4.1. Geometry

The spherical steel ball test consisted of a 15.0" diameter solid steel sphere embedded in a realistic soil. Table 2-1 lists all of the relevant material properties that were used in the analysis. Also included in Table 2-2 is the maximum allowable element size, which is determined by calculating 25% of the shortest wavelength of a propagating wave in the material, i.e., 4 elements per wavelength. Figure 2-1 shows the finite element mesh for the steel ball embedded in soil.

Table 2-1. Material Properties for UXO Finite Element Models

Material	Young's Modulus lb/in^2	Loss Factor	Mass Density (lb/in^3)(sec^2/in)	Poisson's Ratio
Steel	2.85e+07	0.01	7.267e-04	0.31
PBXN-103	6,670.0	0.50	1.635e-04	0.48
Shallow Soil	14899.0	0.02	1.715e-04	0.38

Table 2: Maximum Allowable Element Sizes for Soil Elements

Elsize = Maximum Element Size
C_s = Shear wave speed
λ_{min}=(C_s /frequency) = 4(elsize)
C_s= 5,510.0 in/sec

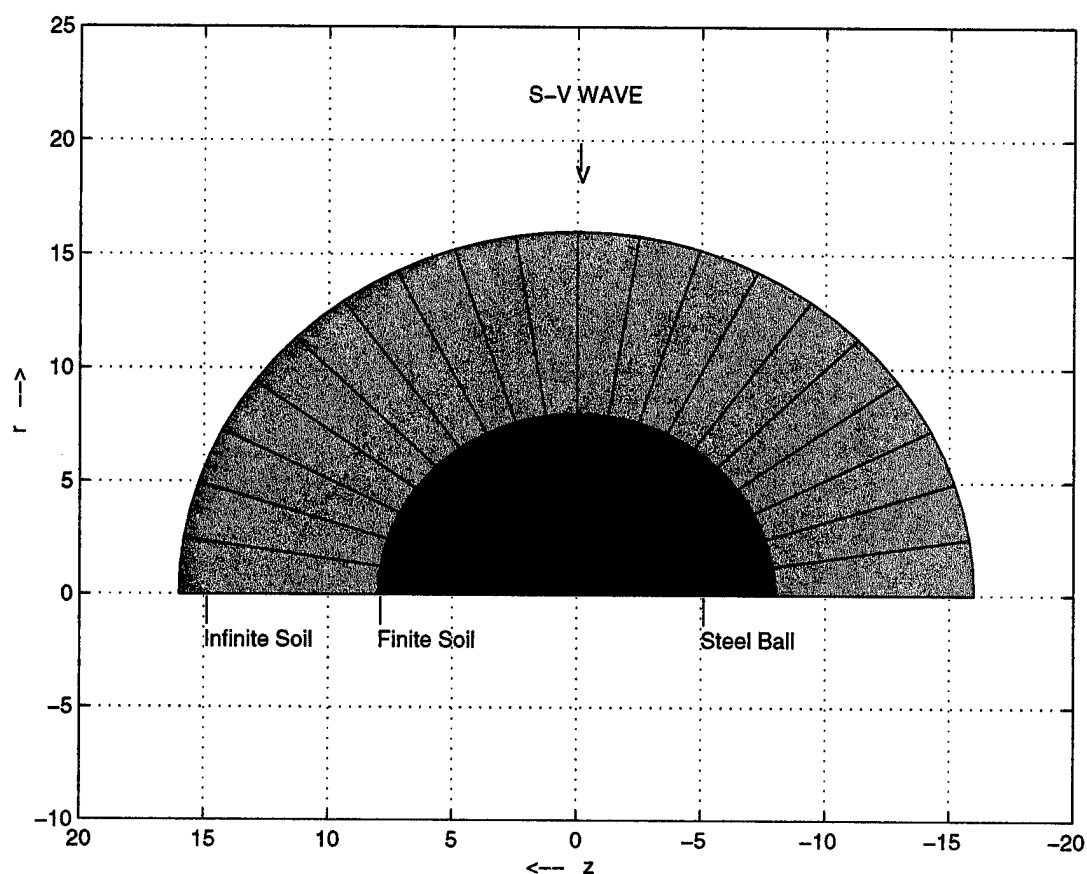| Frequency (Hz)	elsize (in)
100.	13.76
200.	6.88
400.	3.44
800.	1.72
1000.	1.38
2000.	0.69

Figure 2-7. SARA finite element model of steel ball

The mortar shell finite element model consisted of a 155 millimeter projectile, ME, M107. See Figure 2-8 for finite element model layout derived from the U.S. Army Armament drawing number 10535927. The material properties assumed for the mortar shell were steel for the outer shell and material properties for PBXN-103 were used for the explosive core, because these were available. Material properties for soils were derived from earlier field measurements and were used for both the finite and infinite soil elements.

The definition of coordinate system used for axisymmetric finite element modeling is shown in Figures 2-7 and 2-8. The convention is as follows: **r** is defined as the radial coordinate, **z** is along the axis of symmetry, and **phi** is the angle about the axis of symmetry referenced to the positive r axis. A value of **phi**=0 degrees

refers to the **r-z** plane. A value of **phi** = 90 degrees refers to the plane formed by the **z** axis and **r**=0 is out of the plane of the page.
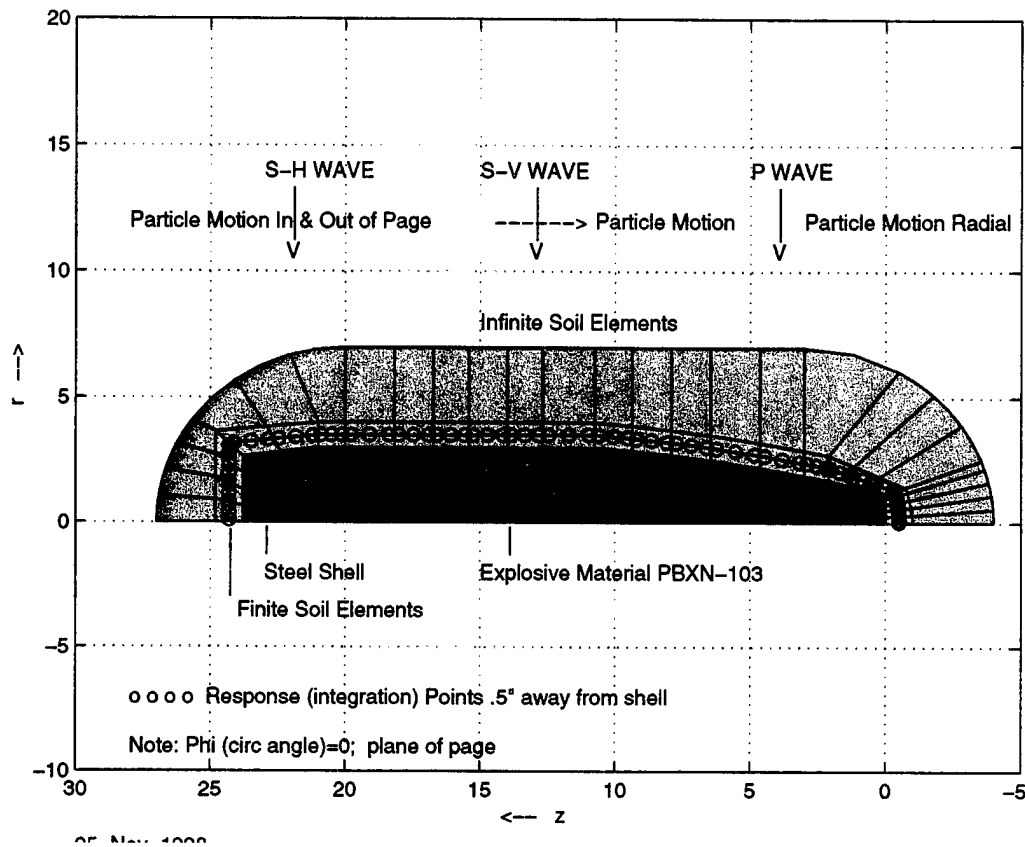

Figure 2-8. SARA finite element model of 155 mm mortar shell with explosive

2.4.2. Loading Conditions

Three wave types were analyzed for the two finite element models.

- P – wave (dilatation wave)
- S - V wave
- S - H wave (Mortar Shell Only).

2.4.3. Calculated Results

The analysis results for the sphere and the mortar shell are found in Figures 2-9 to 2-15. These results are color contours plots generated in MATLAB and in all cases the results are the solutions for displacements at points in the soil 0.5" from the ball or mortar shell surface.

These results are presented as a function of frequency over a range of 0 - 2000 Hz and receive angle for the steel ball. For the 155mm shell the results are plotted as a function of integration point along the mesh due to the uneven spacing in angle of the mesh points. The nearfield calculations have not been completed as of this date.

Results are presented in dB magnitude in displacement inch per unit input displacement for the following cases:

- The sphere for P and SV total displacement

- The 155mm shell SV , total and z axis displacement

- The 155mm shell P , total and r axis displacement

- The 155mm shell SH, total or tangential axis displacement, which are equivalent

Of particular importance to UXO discrimination are the distinct high level modal lines that are present in the response of the 155mm shell. These fall in the range from 1500 –2000 Hz and occur for both P and S incident waves and at different incident angles and polarization.
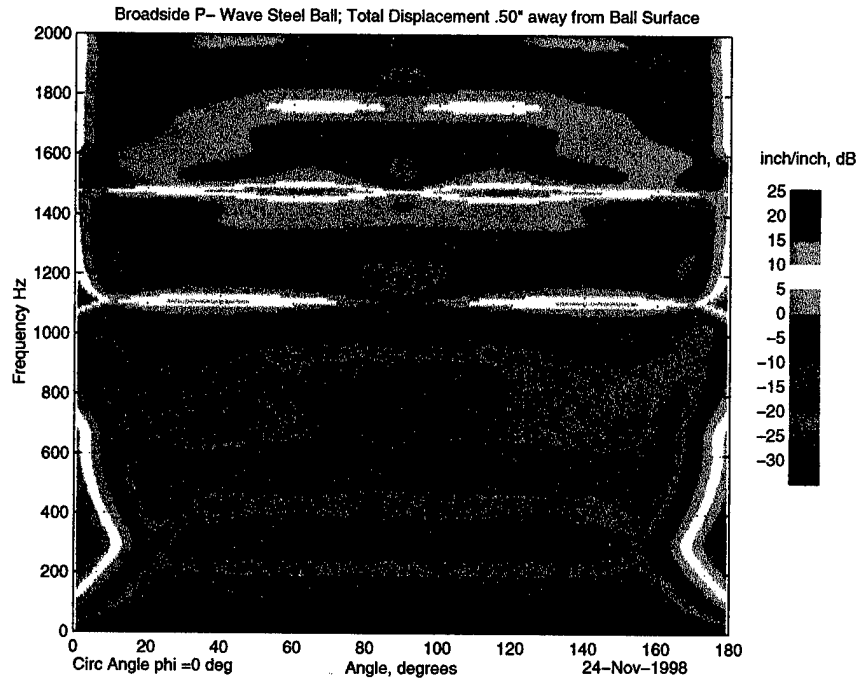
Figure 2-9. Finite Element Analysis Results of Spherical Ball Test Specimen: Broadside P-Wave Load; Total Displacement 0.50" from Ball/Soil Interface in the r-z plane (plane of the page; Phi = 0.0 deg.) vs. Frequency and Receiver Angle
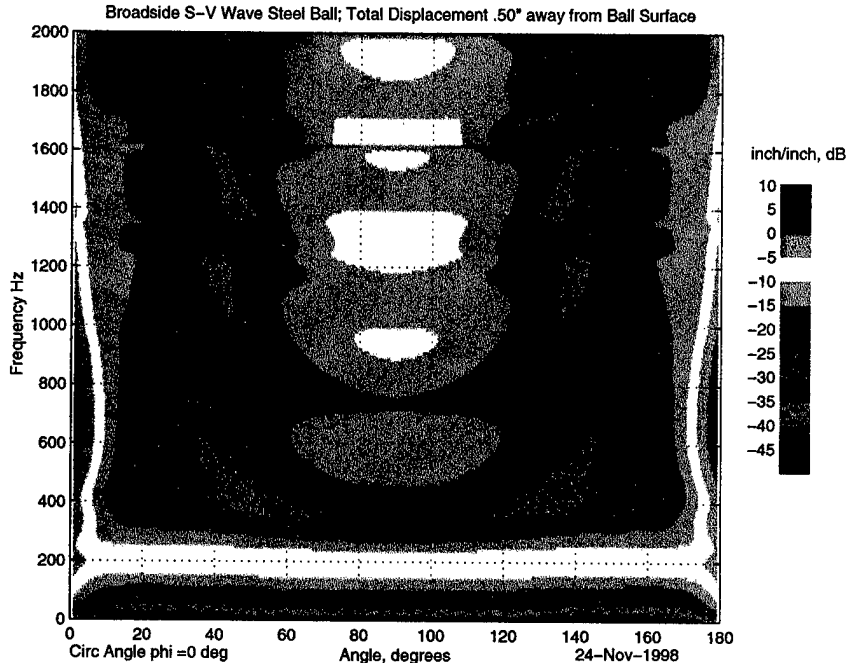

Figure 2-10. Finite Element Analysis Results of Spherical Ball Test Specimen: Broadside SV-Wave Load; Total Displacement 0.50" from Ball/Soil Interface in the r-z plane (plane of the page; Phi = 0.0 deg.) vs. Frequency and Receiver Angle.

Figure 2-11. Finite Element Analysis Results of Mortar Shell: Broadside P-Wave Load; Total Displacement 0.50" from Shell/Soil Interface in the r-z plane (plane of the page; Phi = 0.0 deg.) vs. Frequency and Integration Point.
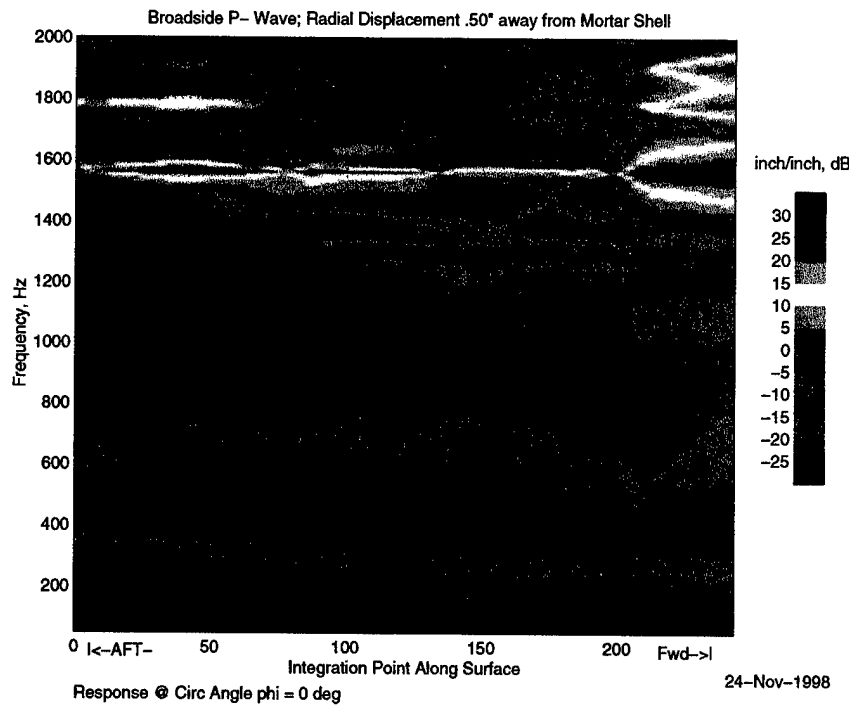
Figure 2-12. Finite Element Analysis Results of Mortar Shell: Broadside P-Wave Load; Radial Displacement 0.50" from Shell/Soil Interface in the r-z plane (plane of the page; Phi = 0.0 deg.) vs. Frequency and Integration Point.
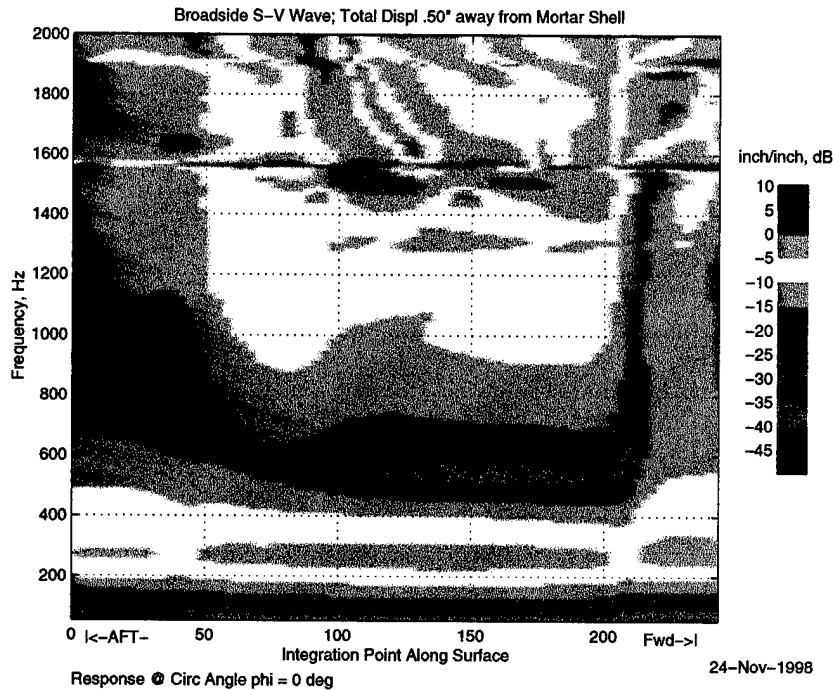
Figure 2-13. Finite Element Analysis Results of Mortar Shell: Broadside SV-Wave Load; Total Displacement 0.50" from Shell/Soil Interface in the r-z plane (plane of the page; Phi = 0.0 deg.) vs. Frequency and Integration Point.
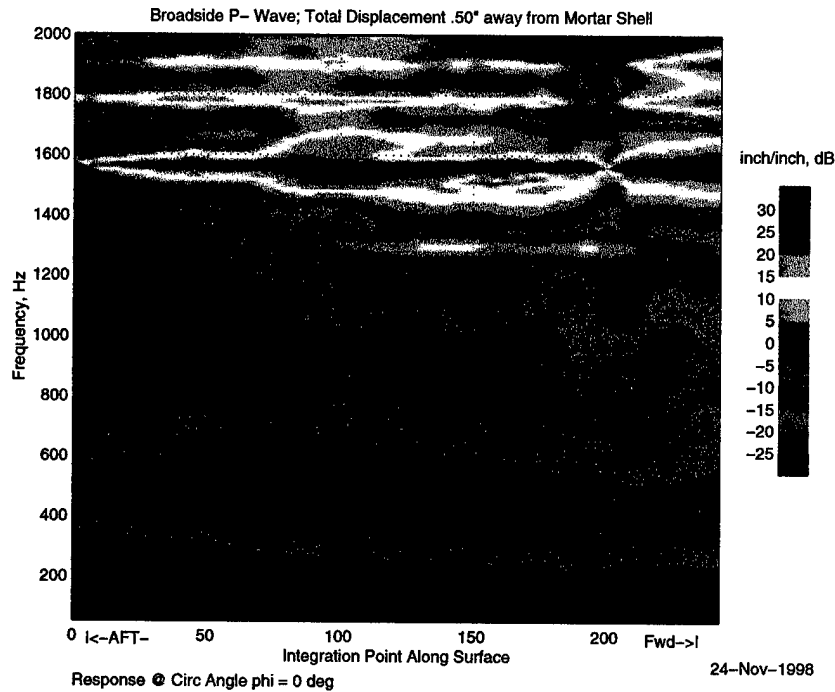

Figure 2-14. Finite Element Analysis Results of Mortar Shell: Broadside SV-Wave Load; Axial Displacement 0.50" from Shell/Soil Interface in the r-z plane (plane of the page; Phi = 0.0 deg.) vs. Frequency and Integration Point.
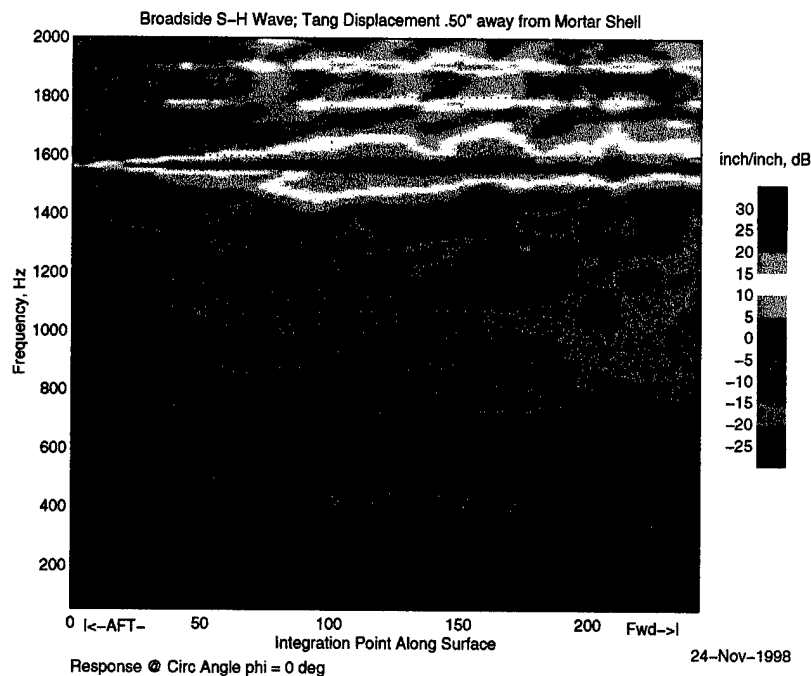
Figure 2-15Finite Element Analysis Results of Mortar Shell: Broadside SH-Wave Load; Tangential Displacement 0.50" from Shell/Soil Interface in the r-z plane (plane of the page; Phi = 0.0 deg.) vs. Frequency and Integration Point.
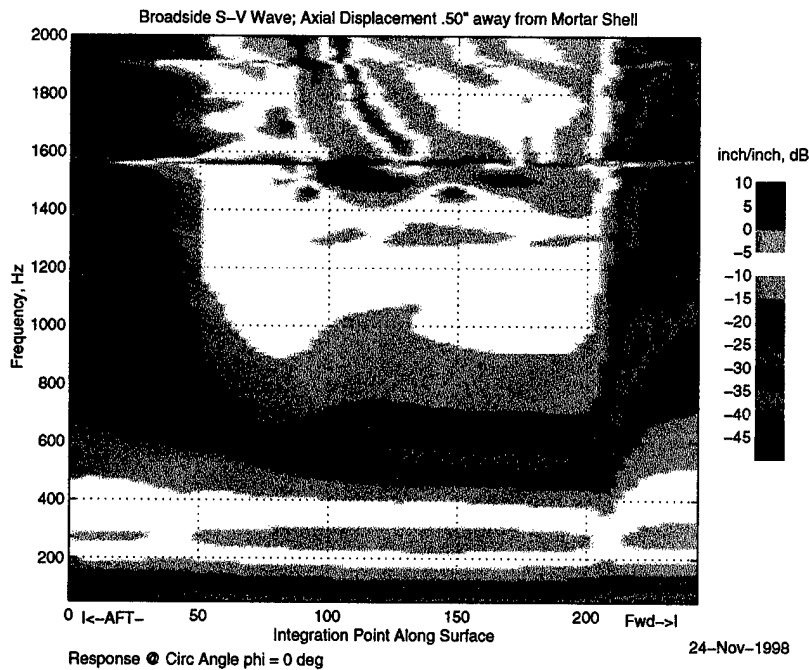
2.4.4. Conclusions of Target Response Modeling

The target strength (TS) of a 15" steel sphere is about –17 dB for shear waves as calculated using analytical methods. The TS has frequency dependence and angle dependence resulting in ±8 dB variation around this value. This TS value can be used for system analysis.

The FEM models show that the displacement field computed just outside the surface of the 155mm shell shows strong modal response characteristics at frequencies in the 1400 to 2000 Hz region. These structural resonances appear distinctive for the different objects. Further validation of the FEM code and refinement of the elastic parameters are needed to confirm these results in the farfield.

2.5. References

2-1. Einspruch, N. G., E. J. Witterholt, and R. Truell. "Scattering of a plane transverse wave by a spherical obstacle in an elastic medium," *J. Appl. Phys.*, 31:806-818, 1960.

2-2. McBride, R. J., and D. Kraft. "Scattering of a transverse elastic wave by an elastic sphere in a solid medium," *J. Appl. Phys.*, 43:4853-4861, 1972.

2-3. Gubernatis, J. E., E. Domany, J. A. Krumhansl, and M. Huberman, "The Born approximation in the theory of the scattering of elastic waves by flaws," *J. Appl. Phys.*, 48:2812-2819, 1977.

2-4. Wu, R., and K. Aki, Scattering characteristics of elastic wave by an elastic heterogeneity. Geophysics, 50:582-595, 1985.

2-5. Bettes, Peter, *Infinite Elements,*, Penshaw Press, UK, 1992.

2-6. Allik, H., et al, "SARA-2D User's Manual, Version 95-3," BBN Systems and Technologies, August 1995.

2-7. Medina, F., and J. Penzien, "Infinite Elements for Elastodynamics," *Earthquake Engineering and Structural Dynamics*, 10(5), 1982, pp. 699-709.

2-8. Yun, Chung-Bang, and Jae-Min Kim, "Axisymmetric Elastodynamic Infinite Elements for Multi-Layered Half-Space," *Int. J. Numerical Methods in Engineering*, Vol. 38, 1995, pp. 3723-3743.

2-9. Chow, Y.K., and I.M. Smith, "Static and Periodic Infinite Solid Elements," *Int, J. Numerical Method in Engineering*, Vol. 17, 1981, pp. 503-526.

2-10. Astley, R. J., G.J. Macaulay, and J.P. Coyette, "Mapped Wave Envelope Elements for Acoustic Radiation and Scattering," *J. Sound and Vibration*, Vol. 170, 1994, pp. 97-118.

2-11. Zienkiewicz, O. C., and R.L Taylor, *The Finite Element Method*, 4th ed., Vol. 1, McGraw-Hill, London, 1991.

2-12. Eringen, A. C., and E. S. Suhubi, *Elastodynamics Volume II Linear Theory*, Academic Press, 1975.

3 Seismic Field Tests

3.1 Introduction

3.1.1 Objectives

The objectives of the seismic field tests were to

- Measure seismic wave propagation. Specifically we wanted to record the seismic wavefield in shallow soil for different types of force inputs, identify the different wavetypes, and measure seismic velocities, (Vs, Vp, V_R) and transmission loss (TL in the sonar equation).

- Characterize the seismic noise, both ambient noise and reverberation from seismic sources (N, REV in the sonar equation).

- Measure transducer performance and define what frequencies can be used to detect UXO. Test transducer coupling and consistency, for both sources and receivers (SL, RS in the sonar equation).

- Measure, in situ, the vibrational response of a 155mm shell to ensonification with seismic waves.

- Measure coherence of signal propagation through the shallow earth.

A seismic system's performance is highly dependent on the environment in which it operates. Both the propagation characteristics and the noise characteristics vary from place to place. Design of a system must be based on an accurate characterization of the seismic environment in which it is to work. In part because it is expensive to build a sufficiently large artificial seismic test facility and also because it is not easy to duplicate a natural soil's physical structure, we perform system tests in natural soils. This is more challenging because natural soils are less homogeneous and ideal results are more difficult to obtain, but the transition to a practical system is more certain. Subsequent system design is based on realistic measured parameters as much as possible rather than theoretical or lab experiments.

Seismic field measurements have been made using various horizontal, vertical, and 2D array configurations to determine wavespeeds, attenuation, and noise. To do this we needed to record as many as 60 channels simultaneously. This requires a high-rate multi-channel data acquisition system with low noise, transducers, cabling, and interfaces.

3.2 Equipment Description

3.2.1 Transducers—Sources

Seismic sources generate waves by applying force to the ground. The different seismic wave types—compressional (or dilatational), shear, and surface waves—are generated differently by applying the force in different ways. The coupling of the energy into the ground is dependent on the size of the contact, the orientation of the force, and the magnitude of force. Impact sources, which impart a high level, short duration force to the ground, were tested as well as controlled frequency swept vibrator sources, which put energy into the ground over a long period. Different methods of applying the force were compared by measuring the resulting wavefield in space with arrays of surface biaxial geophones and downhole triaxial geophones.

3.2.1.1 Hammer Sources

Sledge hammers have been used for a long time as simple, efficient sources for shallow seismic applications. The hammer is swung overhead and hits a steel plate placed on the ground, which sends an impulse into the ground. This is quite effective at generating low frequency energy, but is not very repeatable.

We developed a simple hammer source for making quick direct measurements with an impact source, which provides a more consistent impulse by controlling the geometry of the impact. This consists of a round base plate made of steel, with a solid rod threaded into it. The 4-foot-high rod acts as a guide or slider and is covered with a Teflon tube to reduce friction and sliding-induced vibration. The rod also pushes the base plate to the ground to keep it from bouncing. The hammer is a hemispherical ball of steel with a hole and a tube threaded into it,

which fits over the guide rod. Lead weights were made to fit on top of the hemisphere to increase the weight of the hammer as desired.

For the most consistent impulse with as little bounce as possible, an operator holds the rod and pushes the base plate to the ground. He then lifts the hammer to a particular height and slides it down while holding on to it. After impacting the base plate the operator lifts the hammer up to minimize bounce. This source is effective for applying an impulsive vertical force to the ground.

Figure 3-1. Sliding Hammer Source

3.2.1.2 *Horizontal Traction Source*

A horizontal force produces a different pattern of compressional, shear, and surface waves. To investigate the seismic waves generated by a horizontal source, we tested hitting a specially designed traction plate from the side. This plate consisted of a section cut from a steel I-beam with the web sharpened to a point on one side. This sharpened side is pressed into the surface of the ground and the upright face is hit with a small sledge hammer. This type of source can produce SH waves and surface wave preferentially.

3.2.1.3 *Vibrator Sources*

In earlier work we found that hammers were very simple, reliable sources, but there is little control over the spectrum of energy that goes into seismic waves in the ground. Since the detection of UXO requires short wavelengths and high frequencies, we investigated small vibrators that can be driven with the desired bandwidth signal. We tested two models, a commercially available Wilcoxon F4 shaker and a BBN model MA50 compact vibrator. These sources are commonly used in structural acoustics applications and testing. Relatively small vibrators were used for field testing to develop a set of requirements for a vibrator source. GTE-BBN has a family of larger vibrators as well as capabilities for developing vibrators as necessary.

The Wilcoxon F4 shaker (Figure 3-2) is a compact moving coil device capable of 5-10 lbs. of force over the bandwidth of 50 to 2000 Hz. The shaker is equipped with an impedance head consisting of a force gauge and an accelerometer on the output of the shaker. The shaker is driven by a linear audio amplifier and can be driven with any type of test signal or sweep. As with any electromechanical shaker, the harder it is driven, the more harmonic distortion is present. Information and specifications can be obtained from: Wilcoxon Research, 21 Firstfield Road, Gaithersburg, Maryland 20878 (TEL: 301-330-8811, FAX: 301-330-8873, EMAIL: sensors@wilcoxon.com).

Figure 3-2. Wilcoxon F4 Shaker with force gauge and accelerometer monitoring sensors.

Weighing just 12 pounds, the BBN MA-50 shaker system (Figure 3-3) is just 5"x5"x6" and features 50 lbf continuous and 100 lbf intermittent duty output from 100-2000 Hz. Its high force to weight ratio of 7:1, compactness, and rugged design make it especially well suited to field applications.

Figure 3-3. BBN MA-50 Shaker

3.2.1.4 *Vibrator Ground Coupling Methods*

To efficiently transfer energy into the ground and to efficiently radiate seismic waves, vibrators need to see a high mechanical impedance at their output. The shakers described above put their specified force levels into rigid, high impedance structures. The soil is actually a relatively soft spring, and it is especially soft at the surface. We are testing some different approaches for raising the impedance. The first is by driving the earth over a larger contact area. This is limited by two factors. The mass of coupling device becomes significant, and the source becomes directive as the contact area becomes larger than one-third of the wavelength of the wave in the soil. The second method of raising the impedance is to penetrate the surface soil and apply the force to the stiffer soil below. To do this, we tested 1.5" spikes of different lengths and a wedge approximately 5" by 8", pushed vertically into the soil, with the shaker mounted above ground.

3.2.2 Transducers—Receivers

Conventional geophones used for oil exploration and even shallow surface seismic applications are required to operate only up to a few hundred Hz. Higher frequencies remain difficult to achieve, not because of the transducers themselves but because of the coupling at the interface with the ground. In previous work we developed a system that applies a static weight to the ground, compressing the soil and increasing the stiffness at the contact. This weight is dynamically isolated from the contact disk and transducer, allowing the

transducer to move with the ground at higher frequencies. This system is being evaluated for frequencies above 500 Hz.

A second key receiver issue is the value of recording multiple component ground motion at the same point. By recording the total ground motion in three dimensions, it is possible to select a polarization of the signal of interest and reduce the level of other signals or noise coming from different directions. We used biaxial surface geophones rotated to collect three component surface data and triaxial downhole geophones to test the value of multi-component data.
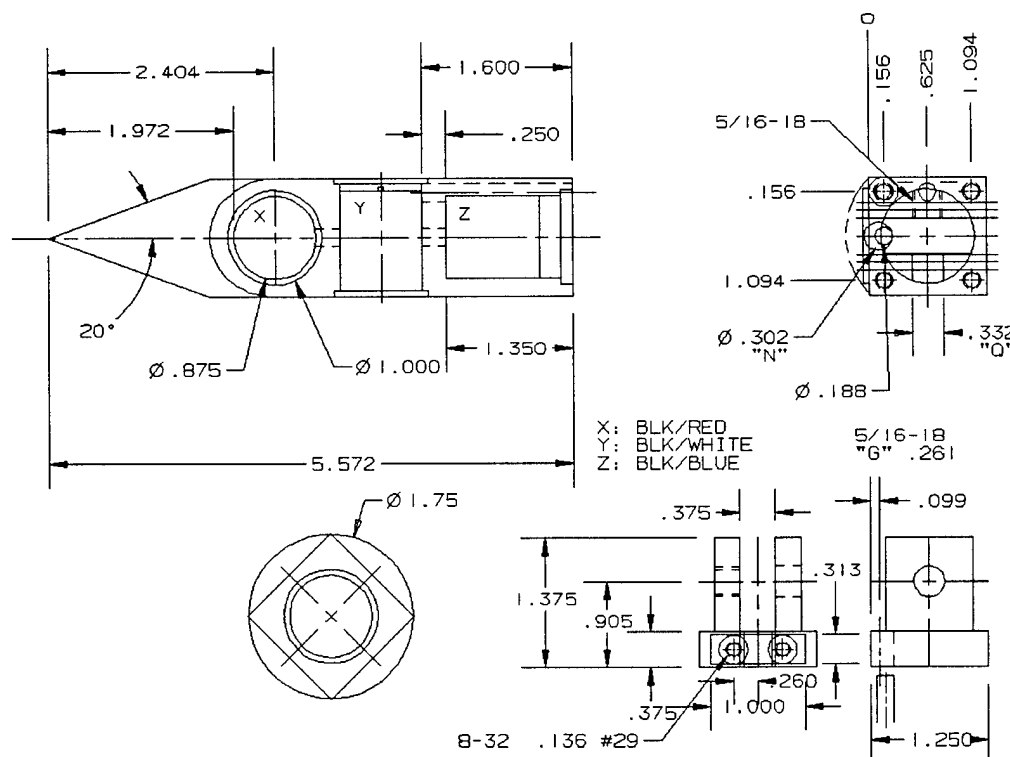

Figure 3-4. Drawing of triaxial downhole geophone with three SMC-70-280 geophone elements.

Additionally there is the issue of the sensitivity and noise characteristics of the transducers themselves, which turn ground vibration into voltage. Commercial geophones are moving coil devices that produce voltage as a function of velocity along the axis of the unit. These geophone units have a spurious resonance in the 600- 1000 Hz range, which can affect data in these bands; the manufacturers do not recommend using them at or above these frequencies. Two units were used in our tests. An OYO Geospace SMC 28-270 (28 Hz, .384 V/in/sec) miniature

unit was used in the triaxial geophone, and an older model Geosource unit SM-11 (30 Hz, 0.76 V/in/sec) was used in the biaxial geophones.

An alternative to velocity sensing geophones is commercial accelerometers made by companies such as Wilcoxon, PCB, and Kistler. These generate voltage proportional to acceleration. These units usually use a piezoelectric crystal and may have a FET built in to preamplify the signal, which requires a power supply for each channel. These are more expensive and not very sensitive at low frequency, but they are excellent high frequency transducers. A Wilcoxon 726T unit was tested, which has a good noise floor and sensitivity specification to over 3 kHz.

A comparison of the noise floor of the two devices is shown below. Above about 500 Hz the geophone has higher noise, at 1500 Hz it is over 10 dB noisier.
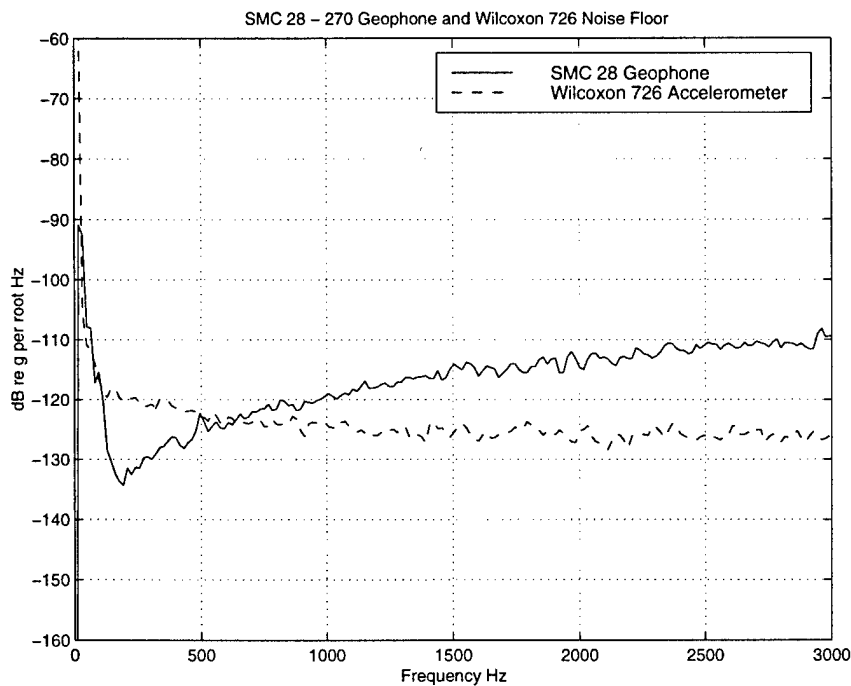

Figure 3-5. Comparison of noise floors for commercial moving coil geophone, Geospace SMC-70-280 and commercial accelerometer Wilcoxon 726-T. Units in power spectral density dB g^2/Hz. The shape of the geophone noise floor is the result of conversion to equivalent acceleration.

3.2.3 Data Acquisition and Measurement Systems

Simple tests of transducers, such as noise floor measurements and source performance and coupling impedance tests were performed with an HP3562 and 35670 dynamic signal analyzers. These have very low analog noise characteristics and also have built-in source waveform generators.

To perform the seismic field testing with arrays of sensors necessary for simultaneously sampling the seismic wave fields, we needed a broad bandwidth multi-channel data acquisition system. For other acoustics programs we have assembled VME-based hardware and software utilities for doing multichannel data acquisition. This system was modified to perform the types of signal generation and acquisition required for tests with both impulsive sources and vibrator sources.

The UXO data acquisition system consists of a bank of 128 analog low-pass filters, a dual backplane VME cardcage, and a Sun SparcStation. A block diagram of the system is shown in Figure 3-6 below.
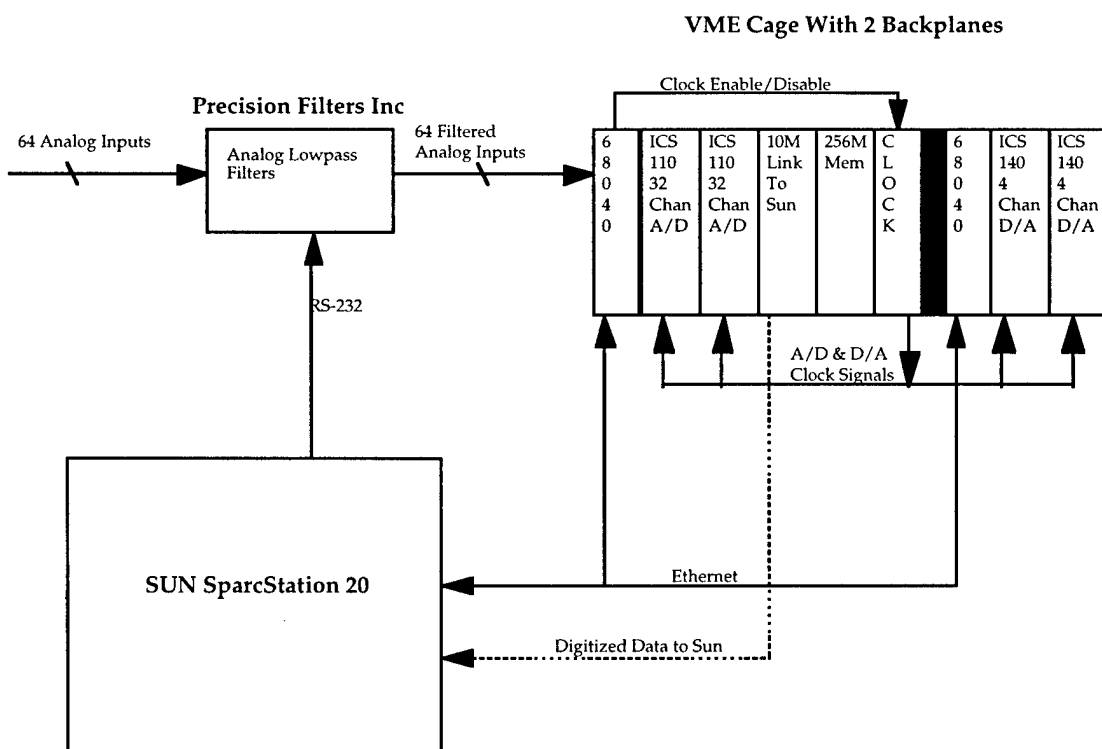

Figure 3-6. UXO Data Acquisition System

3.2.3.1 Analog Filtering

The Precision Filters Chassis with model 6618-LP1-F4-G-M110 analog filter cards provide anti-alias filtering and gain for the A/D input signals and reconstruction filtering for the D/A output signals. The filters are 6-pole, 6-zero elliptic filters that provide 80 dB/octave rolloff. Each channel is independently programmable with four cutoff frequency selections and post-gain selections ranging from 0 dB to 36 dB in 6 dB steps.

3.2.3.2 VME Hardware

The VME cage has two independent backplanes. Each backplane has a Motorola controller card with a 68040 processor running the VxWorks real-time operating system. The input side has five other VME cards used during data acquisition. There are two 32-channel A/D cards, model ICS-110A from ICS (Interactive Circuits and Systems Ltd.), for data acquisition. These cards use 16-bit Sigma-Delta A/Ds that allow for ±2 volt peak input signals. The 256 MByte memory board, model 6390 from MicroMemory, is used to hold the A/D data during data acquisition. The VME bus to S-bus adapter card, model 467-1 from Bit-3, is used to transfer the collected A/D data to the Sun. This card provides a 10Mbyte/second link between the Sun and the VME chassis. The clock board provides simultaneous sampling between the A/Ds and the D/A. This card was custom built by BBN, to convert the oversampling clock used by the Sigma-Delta A/Ds to the clock signal needed for sample and hold type devices. The sample rate set by this board for this system was 10Khz.

The output side has two other cards used during data acquisition. They are the 4-channel D/A output cards, model ICS-140-8A from ICS. The 16 bit D/As can output signals with a peak value of ±10 volts.

3.2.3.3 Workstation Hardware and Operations Control

The workstation is a Sun Sparcstation20 running Solaris with an 8-gigabyte disk and 96MB of RAM. The Sun has overall control of all the hardware. It communicates with the processes running on the 68040s via Ethernet. It controls the setting of analog filters via an RS-232 serial port.

There is a GUI (Graphical User Interface) written in Tk/Tcl that runs on the Sun that controls the acquisition of data, which signals get sent to the shaker, and the gain and filter settings for the analog filtering.

3.2.3.4 Other Equipment

This computer equipment, plus the analyzers, sources, receivers, interface cabling, and tools required were loaded in a 15 foot rental truck (Figure 3-7). Tests were performed with the equipment set up in the truck and cables leading to the geophone arrays. A 4-KW gasoline generator was used to power the computer and instrumentation. The generator was placed on a tire and placed over 100 feet from the test site to reduce any vibration input to the ground. Though the generator was grounded and the truck was grounded, there was residual electronic noise at 60 Hz and harmonics out to 1000 Hz.
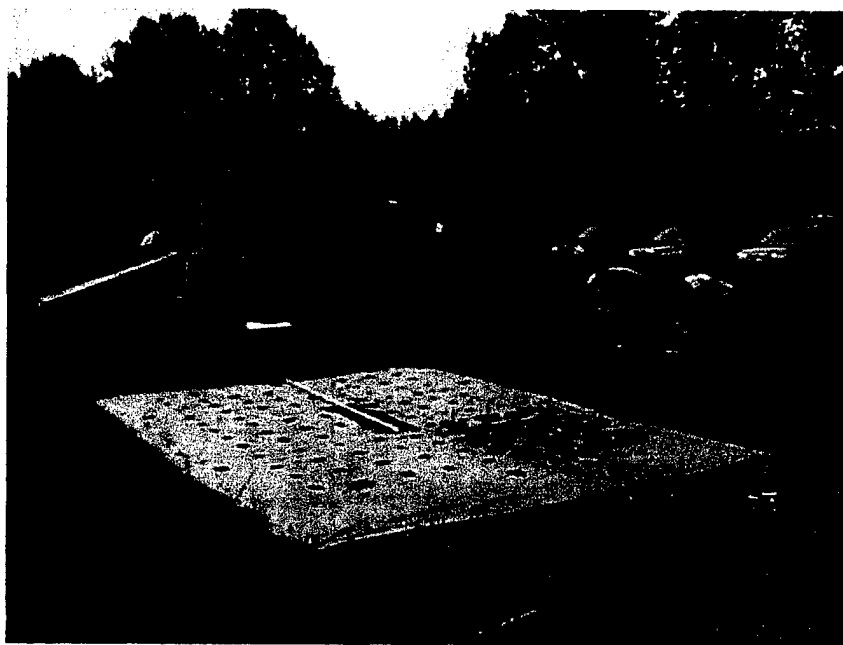

Figure 3-7. Picture of test site with geophone array and truck with data acquisition equipment.

3.3   Test Site Description

We performed initial transducer and propagation tests at our offices in Cambridge, Mass. This soil is primarily compacted construction full and very heterogeneous.

For our more extensive tests, we looked for a test site that would offer a relatively homogeneous, simple seismic environment. We do not consider it cost effective at this time or realistic to construct a "sandbox" for testing, because it would have to be large to make a low reverberation environment and would not have realistic seismic properties. Also, our goal was to test seismic system components as well as to measure seismic velocities, attenuation, noise, and reverberation in a natural environment.

We looked for a site nearby our offices in Cambridge with a natural soil with few rocks and minimal soil layering. A fairly smooth and level site facilitates this type of field work, but we did not want a site that was graded or made with construction fill. A site with minimal vegetation is also more convenient for operations. Since we wanted to test propagation below the surface, we wanted a site that was easy to dig in for placing downhole receivers and burying a shell to test its response to seismic waves.

I had hiked along the Souhegan River in my home town of Amherst, N.H., and knew from examining the banks that the deposits were primarily fine silts and clays. I inquired about performing tests at land along the river and was led to an unused farm field with vehicle access for a landing on the river. Permission was obtained from the town conservation commission.

The field was no longer being farmed but was regularly cut for hay. There were slight remnants of furrows, probably from plowing long ago. The land was bordered on one side by a road with moderate traffic and on another side by the river. Otherwise there were no other buildings or activities for about a half mile.

A test hole revealed a surface layer of roots and dark brown-black stained soil 4" to 6" deep over a relatively homogeneous brown-orange soil of clay and fine to medium sand. With a post-hole digger, I easily dug to about 3 feet deep. The walls of the hole did not cave in at all. No rocks were encountered. The soil was

moist but not saturated, and it held together when compressed in the hand, but was not clayey enough to be able to roll into a ball.

*Figure 3-8. New Hampshire test site soil composed of fine silt and sand.*

3.4 Field Methods and Results

Sources and geophones were laid out on the surface in different patterns to measure seismic wavetypes and reverberation. We conducted the following primary experiments:

- Radial Line Refraction Experiments

- Downhole Geophone Measurements

- Coherence Measurements

- 2D Array Experiments

- Buried Shell Response Measurements

Many experiments were repeated using the different sources and different source receiver geometries. Extensive analysis has been done and is continuing on these experiments. A description of the experiments and examples of the results are presented here. An example of the map of the geometry of sources and receivers for a day of experiments is shown in Figure 3-9. The map for this day included

geophone arrays for the radial line, downhole measurements, coherence measurements and buried shell response measurements.

Souhegan Field Test 2 - Closely Spaced Array Test

Figure 3-9. Geometry for New Hampshire Field Tests
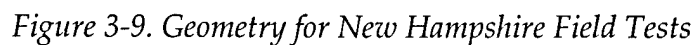
3.4.1 Radial Line Refraction Experiments

To measure seismic velocities and attenuation, the standard geophysical technique of seismic refraction was used, but at a much reduced scale than is typical. This method measures seismic velocities by analyzing the waves propagating away from the source, to geophones placed at evenly spaced increasing distance on the surface. We placed the biaxial geophones at a 1-foot spacing starting 1 foot from the source out to 16 feet from the source. After recording 16 ground positions, we shifted the geophones out to from 16 to 31 feet from the source, with one geophone ground position overlapping with the previous line.

All the source coupling experiments were performed using this radial line array. An example of data with the sliding hammer source is plotted in Figure 3-10. Each trace has been normalized separately so the relative amplitude is not displayed. The earliest arrival on each geophone is the compressional P wave traveling nearly horizontally near the surface. At this site it has a velocity of 190 meter/second. Also clearly apparent is the Rayleigh wave, which travels at about 105 meters per second. In some areas it is possible to also detect a refracted shear wave separate from the Rayleigh surface wave, but not at this site. At this site we can estimate a shear velocity of 117 m/sec from the Rayleigh wave using an assumed Vr to Vs ratio of 0.9. The transmission loss and attenuation of the Rayleigh wave was also measured and found to be 1.1 dB/ft over the cylindrical geometric spreading. The center frequency of this Rayleigh wave data is at about 250 Hz.
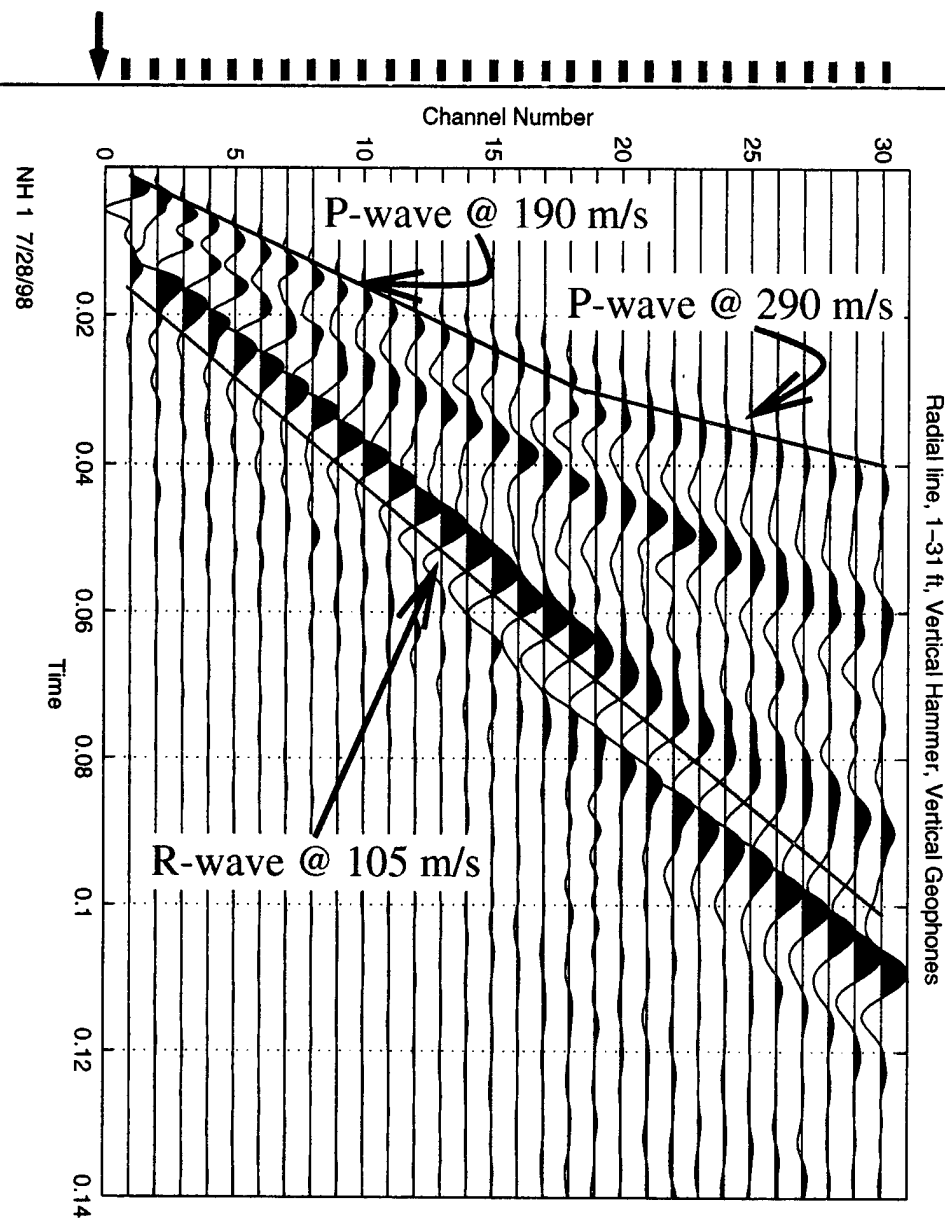
Figure 3-10. Refraction line with geophones at 1-foot spacing. P-wave, refracted P-wave, and Rayleigh wave velocities measured.

3.4.2 Downhole Measurements

Three triaxial geophones were put at different depths in the ground, as shown in the earth cross section view in Figure 3-11. Sources were then placed at different points on the surface to provide different paths at different angles to the downhole receivers. This allows measurement of the seismic wave types and

velocities traveling down into the ground to positions where ordnance would be detected. Additionally, we used this geometry to measure the source bandwidth being transmitted to objects below the surface.
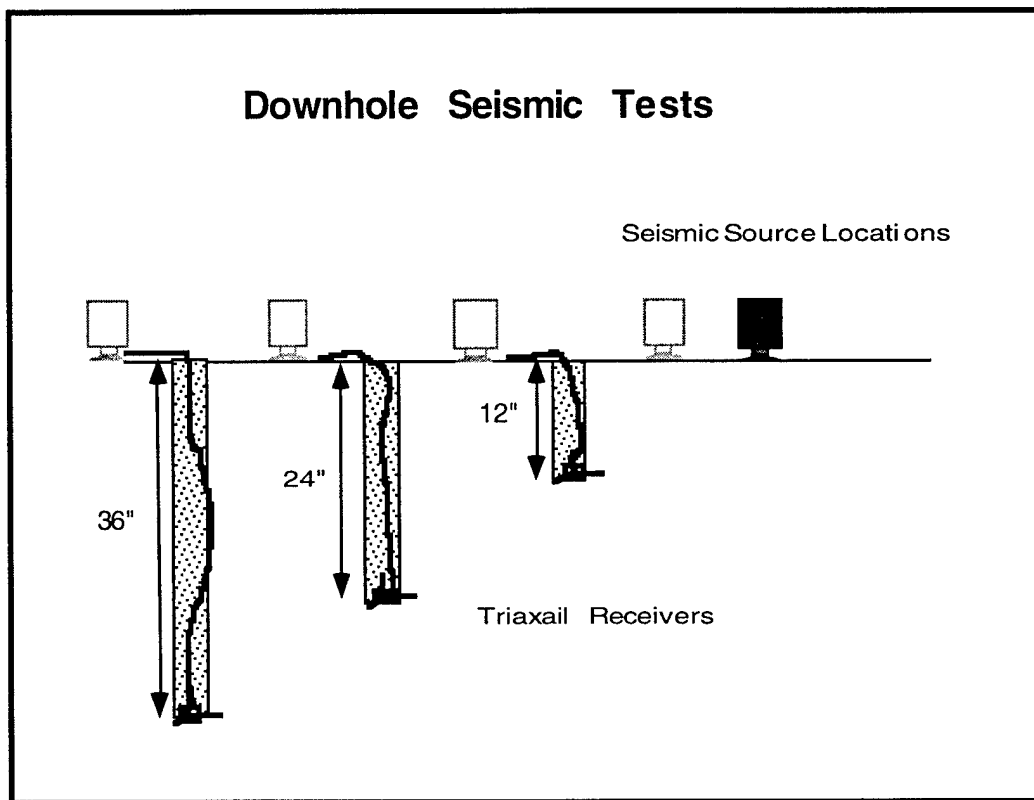

Figure 3-11. Earth Cross Section View of Downhole Geophone Geometry

Figure 3-12 contains plots of the Z components of the signals recorded at the three triaxial phones using the MA50 shaker transmitting a sweep from 200 – 2000 Hz on the surface at the darkened source location in Figure 3-11 above. The vibrator data has been processed to show the time impulse response after the transfer function of the source has been removed. The first arrival of small amplitude is the P wave. Drawing a line along the first breaks and using the distances between the downhole sensors gives a velocity of 196 m/sec. This corresponds well with the P wave velocity measured with the refraction line. Later on each trace, the highest amplitude spike is most likely the shear wave arrival. Again, drawing a line along the arrivals gives a velocity of 107 m/sec. The estimate from the Rayleigh wave velocity measured on the surface was 117 m/sec.
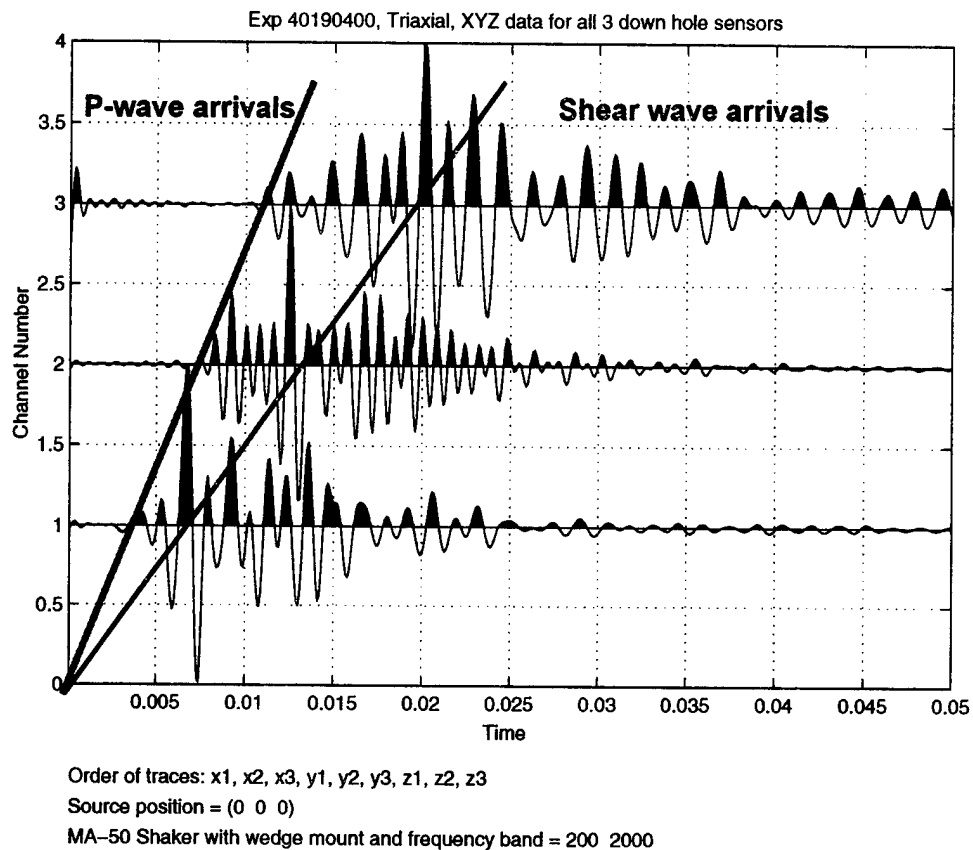
Figure 3-12. Arrivals on z component of three-axis downhole geophones for source on surface.

A comparison of source bandwidths is shown in Figure 3-13 for the hammer source and the MA50 vibrator source with a wedge foot coupling. The spectra show that the hammer source energy is limited to less than 800 Hz, where the spectrum reaches a minimum before it is dominated by sensor noise. The MA50 source extends up to 1500 Hz and above. At 1500 Hz the size of the triaxial geophone is large compared with the shear wavelengths, so the sensor becomes insensitive to higher frequencies. A small single accelerometer placed two feet deep in the ground recorded shaker energy up to 2000 Hz.

Figure 3e, Experiment ID: 40010113
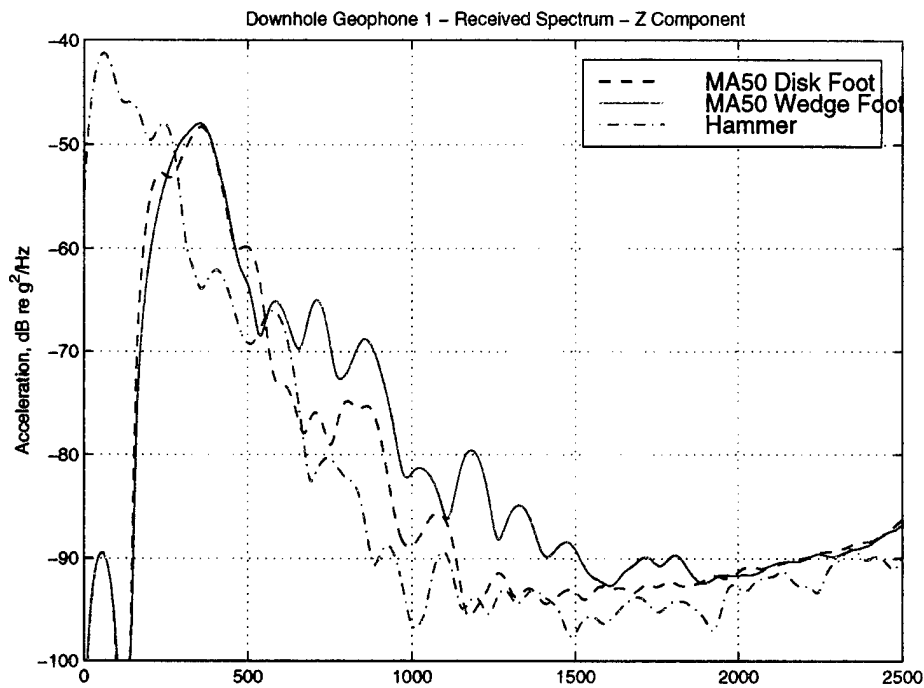Source Position: (0 0 0), Receiver Position: (2   0   1.1667)

Figure 3-13. Receive power spectral density on downhole geophone for hammer source, MA-50 source with disk foot, and MA-50 source with wedge foot.

3.4.3 Coherence Measurements

To evaluate the coherence of paths to buried objects we did a test with a series of ten source locations at equal distance from a downhole triaxial geophone. By looking at how these time traces add up, we can assess how well the beamforming will provide signal gain over different paths through the ground.

Figure 3-14 shows data taken with the MA50 source with the disk foot sweeping from 100 to 1600 Hz at ten different locations on a 5-foot radius from the top of a hole with a triaxial geophone at 36″ below the surface (see arc of source locations on Figure 3-9 geometry) . The ten individual traces have similarities and differences. These differences can be due either to differences in the media along the propagation path or differences in source coupling at the surface. The bottom trace is the sum of all the traces, normalized by the square root of 10 Field Tests. It can be seen that a sharp peak occurs corresponding to the arrival time of the shear wave. Other signals at different times are attenuated relative to this

peak, indicating that coherent shear wave energy is reaching the downhole and that other arrivals of reverberation are attenuated. This is being further analyzed quantitatively.
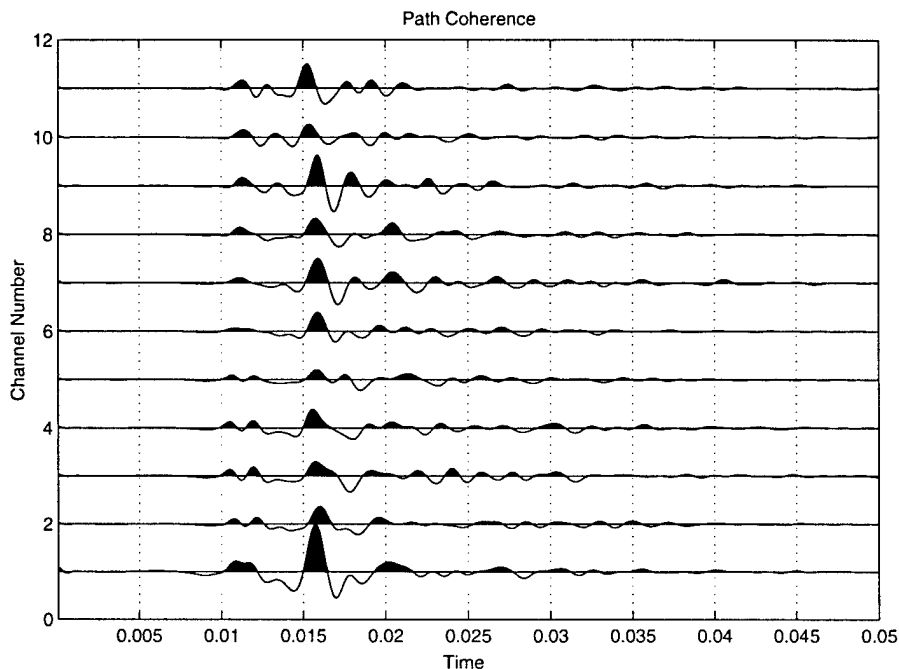

Figure 10, Frequency Band: [100 200 800 1600]
The geophone data see above, has been converted to
acceleration and normalized to the shaker accelerometer.
The first channel above is the sum divided by sqrt(10).

Figure 3-14. Coherence test − plot of ten source locations equal distance from downhole geophone. Bottom trace is stack of all ten normalized by square root 10.

3.4.4   2D Array Experiments

A 2D surface array of geophones was laid out using a template to investigate imaging with a large array. Data was collected with the hammer source at eight source locations with 16 geophone subarrays as shown in Figure 3-15. A full set of array data was acquired with nothing buried. Then a 155 mm projectile was buried 1 meter deep in the middle of the array and the full array of data was collected again. Attempts have been made to image the target with this data but they have not been successful yet. We are continuing to analyze this data set and are looking at problems of spatial aliasing, source reverberation, coherence, and source repeatability with the hammer.
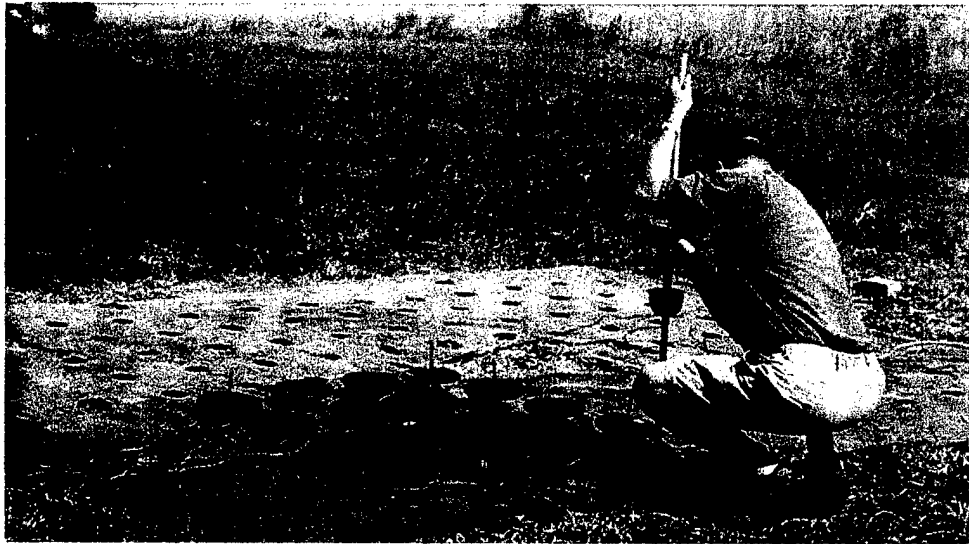
Figure 3-15. 2D array test using hammer source and 16-element geophone subarray.

3.4.5 Buried 155mm Shell Response

We acquired a 155mm shell filled with paraffin from the UXOCOE office. We attached four accelerometers on the top, sides, and tail of the shell (Figure 3-16). The shell was then buried in the ground at a depth of 1 meter (Figure 3-17). The buried shell was excited from the surface with two broadband seismic sources, the sliding hammer and Wilcoxon F4 vibrator. The sources were placed at different relative locations to the buried shell to ensonify the shell from different angles. Time series signals were recorded for each source.
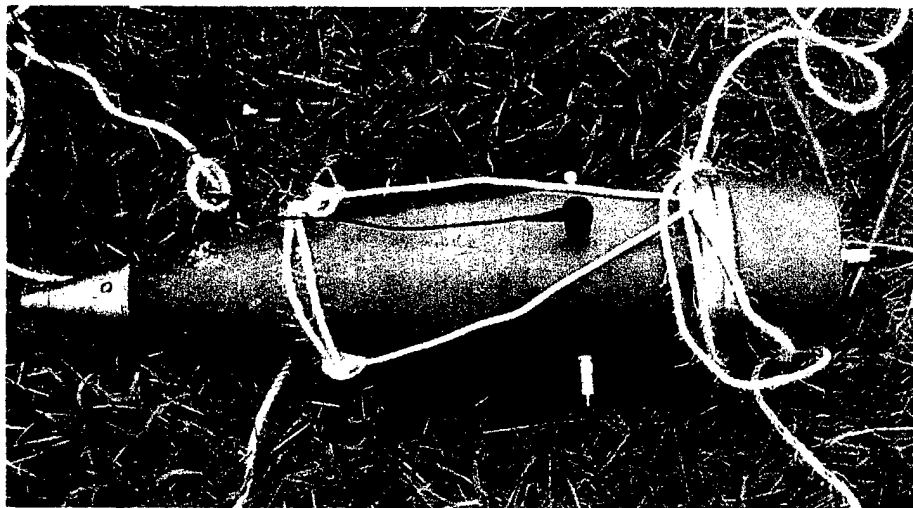
Figure 3-16. Accelerometers attached to 155-mm shell before burial in hole.

Figure 3-17. Burial of 155-mm shell at one meter depth.

The data from the accelerometers on the buried shell was analyzed by computing the transfer function from the accelerometer on the foot of the shaker to the accelerometers mounted on the shell. This normalizes the response to the shaker output. Significant response was seen on the shell up to 1800 Hz, as shown in Figure 3-18. Of particular interest, the spectrum of the shell response shows a prominent narrow peak near 1500 Hz. A similar peak was predicted in our work with our Finite Element Model of the seismic response of a 155-mm shell. This

spectral peak could be used as a seismic "fingerprint" of an unexploded 155-mm shell to distinguish it from fragments.

Surface vibrator source
200-2000 Hz sweep

Accelerometer response on top and side of
155 mm shell buried at 1 m depth
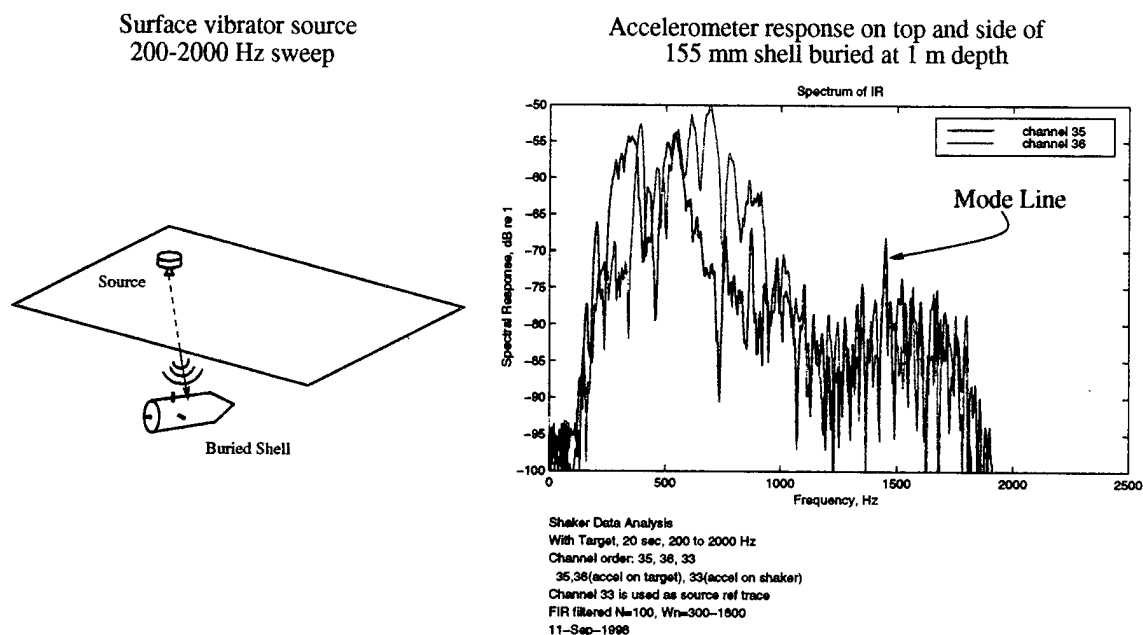
Figure 3-18. Transfer function of response of shell with respect to accelerometer on shaker on surface. Note presence of modal line at about 1500 Hz similar to that predicted with finite element modeling.

3.5 Seismic Field Test Conclusions

3.5.1 Transducer Evaluations

Small portable seismic sources were tested for bandwidth and source strength for UXO detection. Sources tested include vertical and horizontal hammer sources and 2 small vibrators. A sliding 12 lb. impact hammer source was fairly repeatable but has most of its seismic energy at frequencies less than 200 Hz and limited bandwidth confined to the range below 900 Hz. The horizontal hammer source generated high levels of surfaces waves compared with body waves.

A compact MA50 vibrator source with 10 lbs. force output to the ground was capable of putting out more high frequency power than the hammer at frequencies over 300 Hz. It was capable of generating seismic waves in the ground up to 2000 Hz.

Significant improvements in high frequency source coupling of seismic waves can be achieved by penetrating the soft soils surface and increasing the contact area.

Commercially available moving coil geophones can be used up to above 1 kHz without signal degradation and are comparable to accelerometers. The geophones have a higher noise floor than commercially available accelerometers at frequencies above 500 Hz, and they are also more susceptible to 60 Hz pickup.

Three component geophones were developed for downhole placement. These were successfully used for testing of sources and testing algorithms for separation of wavetypes. The three components were successfully used to steer for different polarization wavetypes at frequencies below 500 Hz. Their response appeared to roll off above 1200 Hz, most likely due to the size of the geophone being comparable to the wavelength.

3.5.2   Seismic Wave Propagation

Seismic wave propagation was measured at our Cambridge offices and at a test site in southern New Hampshire.

At our offices, the soil is made up of compacted construction fill overlain by grass. Using a horizontal traction source, we measured a shear wave velocity of about 240 meters/second for the soil near the surface. Using a short spacing refraction line we measured a P wave velocity of 600 meters/second near the surface. A small vibrator with about 0.3 lb. force was capable of generating significant energy above sensor noise floor in the ground in the 1000-2000 Hz band

At the New Hampshire test site, the refraction line experiment showed that P wave velocities were 190 m/sec near the surface and Rayleigh wave velocities were approximately 105 m/sec at 150 Hz. From the Rayleigh wave velocities, shear velocities were estimated to be about 116 m/sec. These velocities were confirmed with measurements from the surface to a set of downhole geophones. Shear wave attenuation was estimated to be 1.1 dB/ft at 250 Hz from both downhole measurements and estimates from Rayleigh wave attenuation. A

vibrator seismic source was tested at this site which generated significant energy above sensor noise floor up to 1800 Hz.

3.5.2.1 Ambient Noise

Ambient noise at both test sites was low compared to sensor noise above 500 Hz. At 200 Hz, the ambient noise power spectral density measured on a moderately windy day was −116 dB re $1g^2$/Hz and it gradually increased at lower frequencies. Comparison of sensors on the surface and buried to a depth of 16" show that ambient noise is primarily confined to the surface, which indicates that for our band of interest, the noise is acoustically coupled or primarily surface waves.

3.5.2.2 Buried 155mm Shell Response to Seismic Waves

Accelerometers were mounted on a 155mm shell and then the shell was buried 1 meter in the ground. A seismic source on the surface was used to excite the shell. A distinct modal resonance frequency showed up near 1500 Hz. This frequency line is similar in frequency to that predicted using the elastic Finite Element Model. This characteristic resonance in the seismic response could be useful in discriminating UXO from other irregularly shaped non-UXO.

4. System Simulation/Performance Prediction

4.1. Introduction

This section describes our efforts to develop a system simulation and testbed for analyzing signal-to-noise ratio and for use as a system design tool. Our work to date includes the following areas:

- Predicting particle accelerations in the far field of a vertical or horizontal source.

- Simulation of synthetic data by calculating travel times from source to a cylindrical target and then to receiver in a homogeneous medium.

- 3D imaging of 2D arrays of seismic data

4.2. Predicting Particle Accelerations

Predicting particle accelerations due to mechanical source excitation is an important part of designing a seismic unexploded ordnance (UXO) detection and classification system. In particular, the engineering design requires the construction of a receiver array capable of recording seismic data that can be usefully processed. Consequently, it is essential to determine whether there is sufficient signal-to-noise ratio (SNR) at the receivers so that the desired processing can be successfully applied.

The SNR of a received signal can be determined by applying an appropriately modified version of the sonar equation. The sonar equation accounts for the source strength and directivity, the round trip propagation effects, the impedance characteristics (i.e., reflectivity) of the target, and the directivity of the

receivers. All these components are evaluated in the sonar equation to arrive at a final estimate of SNR. This section describes the programs written that permit the evaluation of the first part of the sonar equation, that is, the source directivity and a first-order analysis of the source-to-target propagation effects. The medium of propagation is assumed to be an elastic half space. The source is taken to be either a vertically or horizontally applied harmonic force acting on a circular disk of finite radius.

4.2.1. Problem Formulation

The geometry of the source is illustrated in Figure 4-1 for the case of a vertically applied force (left side) and a horizontally applied force (right side). It is assumed that the force is applied to the surface of a rigid disk of radius a..
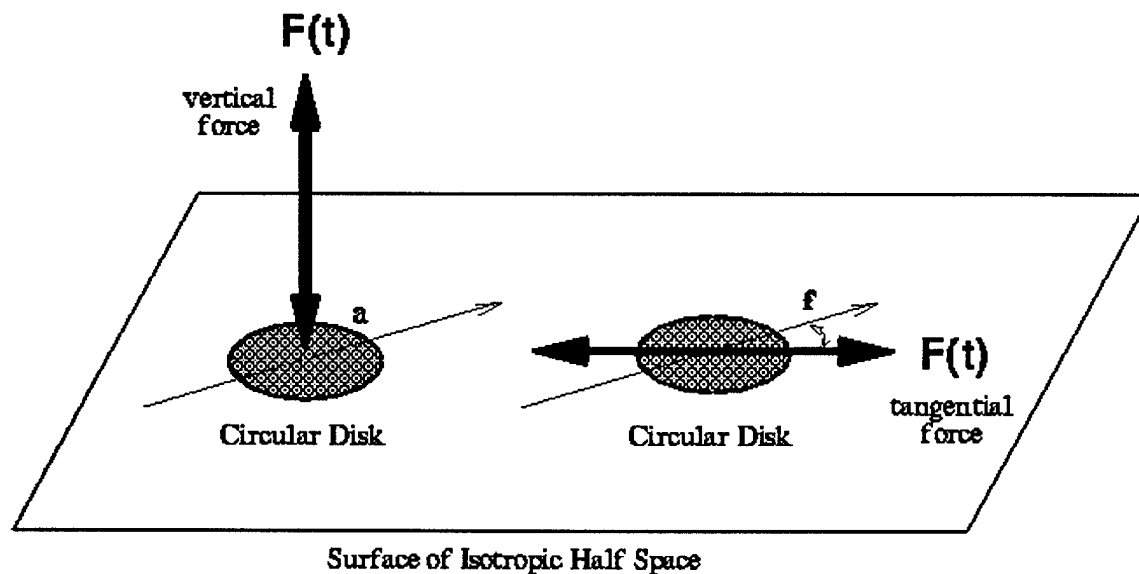
Figure 4-1. Physical Geometry of the Source: The circular disks illustrate the contact of the source with the earth ,and the force vectors illustrate that the force is applied either vertically or tangentially to the earth's surface.

Furthermore, the source is presumed to act on the surface of a semi-infinite elastic half-space. The half-space is presumed to be a linearly isotropic elastic medium which can be completely described by three elastic parameters and an attenuation factor. Usually, the elastic parameters will be taken to be the

compressional and shear velocities, V_p and V_s and the density, ρ. The attenuation is denoted by Q.

4.2.2. Nature of the Solution

The results obtained for predictions of the particle accelerations incorporate a certain number of assumptions and properties. First, the solutions are approximations that are only accurate in the far field. Furthermore, the solutions take into account the different types of particle displacements (compressional, horizontal shear, and vertical shear), account for the attenuation of the medium, and perform a mass correction that accounts for the loading of the source on the elastic half space. The equations used to implement the solution are found in Ref. [4-1].

4.2.3. Examples

In this section several examples are given that illustrate typical results of our prediction programs. These examples compute the mass-corrected far-field particle accelerations with attenuation for a vertically acting source.

The illustrated results are for a vertical 10-pound force (i.e., 44.5 Newtons) applied at a frequency of 1400 Hz to a half-space with V_p = 320 m/s, V_s =140 m/s, ρ =1900 Kg/m^3 and Q = 50. For this problem the source gives rise to particle accelerations that are cylindrically symmetric around the axis of action of the source.

Figure 4-2 illustrates the amplitude of the particle accelerations due to the compressional wave. The source is applied to the upper left-hand corner of the figure and the x and z axes are the usual spatial variables in units of meters. The color bar indicates the amplitude of the acceleration with respect to 1μg. It is important to note that the values are only valid in the far field, which is why the

figure also shows the position of the phase front, which corresponds to 10 wavelengths from the source.

Figure 4-2. Compressional Particle Acceleration due to Vertical Force: The source is located in the upper left-hand corner of the figure and the compressional wave particle accelerations as a function of spatial position are color coded by the colorbar on the right.

Figure 4-3 shows the results of the SV wave particle acceleration for the same parameters as in Figure 4-2. The null between the two main lobes of the source pattern occurs at a critical angle that gives rise to a phase change from one lobe to the other. It should be noted that for a vertically applied force, no SH waves are created.

S—wave Acceleration for Vertical source

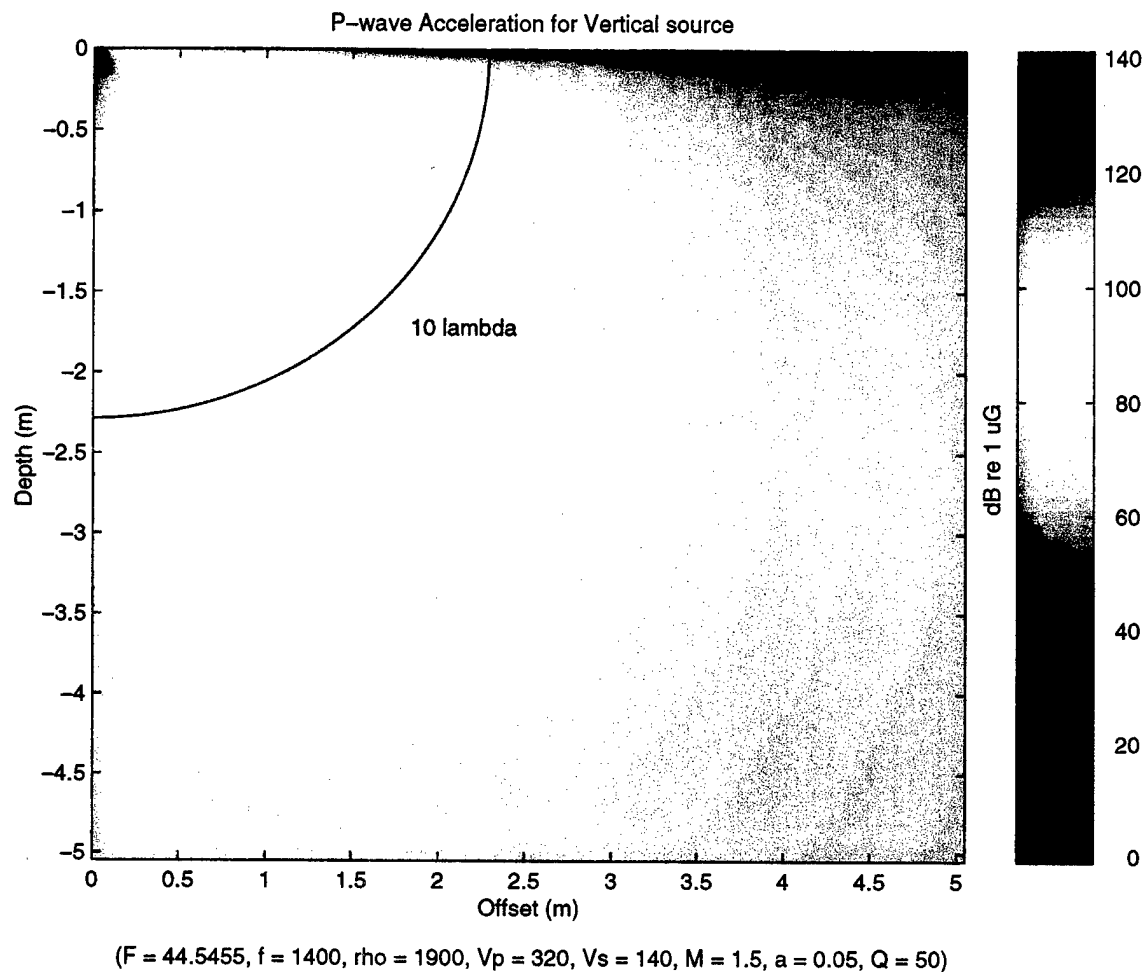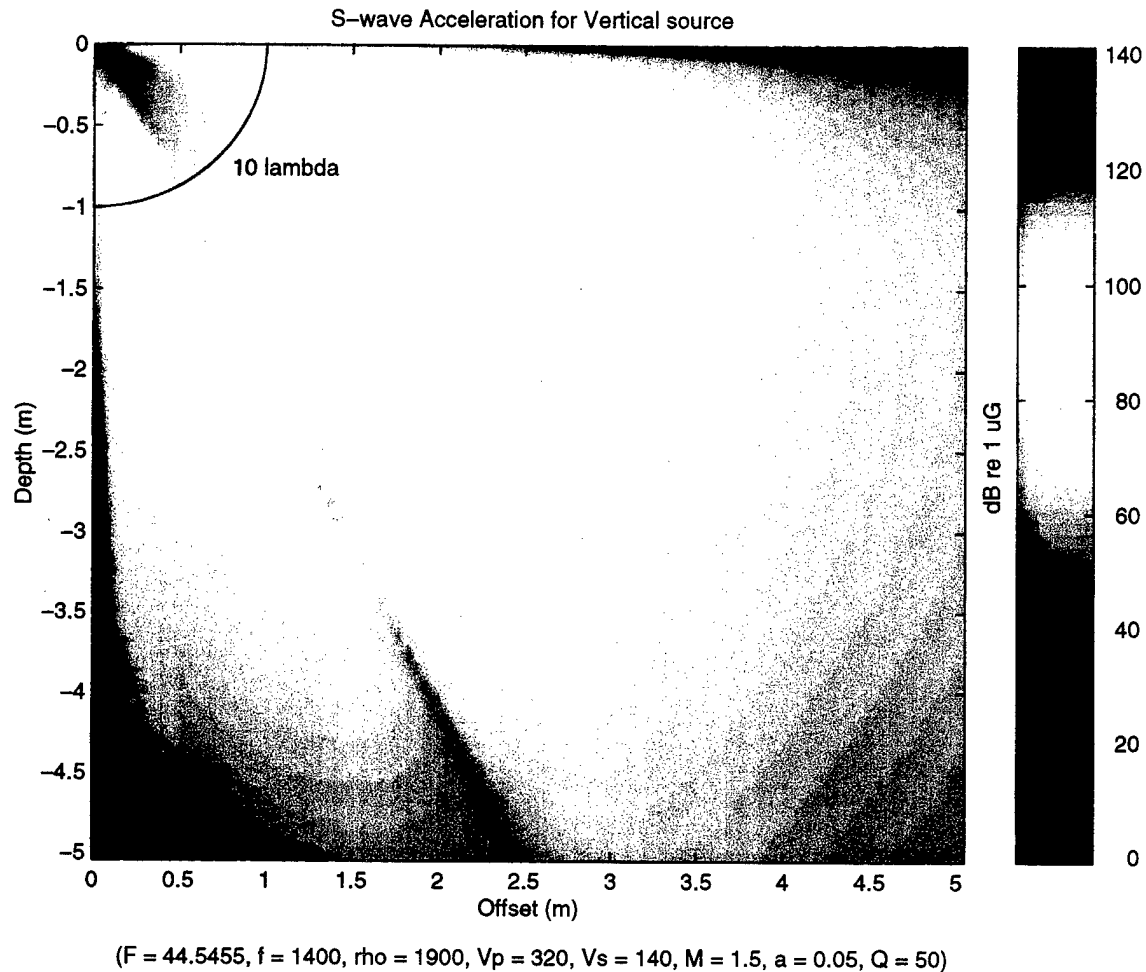(F = 44.5455, f = 1400, rho = 1900, Vp = 320, Vs = 140, M = 1.5, a = 0.05, Q = 50)

Figure 4-3. Shear Particle Acceleration due to Vertical Force: The source is located in the upper left-hand corner of the figure and the shear wave particle accelerations as a function of spatial position are color coded by the color bar on the right.

4.2.4. Comparison to Real Data

This section compares the outputs of the particle acceleration prediction program with results from field data collected at the New Hampshire test site.

The top of Figure 4-4 illustrates the recorded amplitudes of geophone at the earth's surface a few centimeters from the source. The geophone values in units of velocity have been converted to units of acceleration so that they may be compared to the outputs of the prediction programs. The bottom part of the figure illustrates the response of four accelerometers at a horizontal distance of 8

feet from the source and at a depth of 3 feet. The peak values of the two plots are

135 and 106 dB re 1μg.

Trigger Channel

Peak Value = 135 dB re 1μ g

4 Target Channels

Peak Value = 106 dB re 1μ g
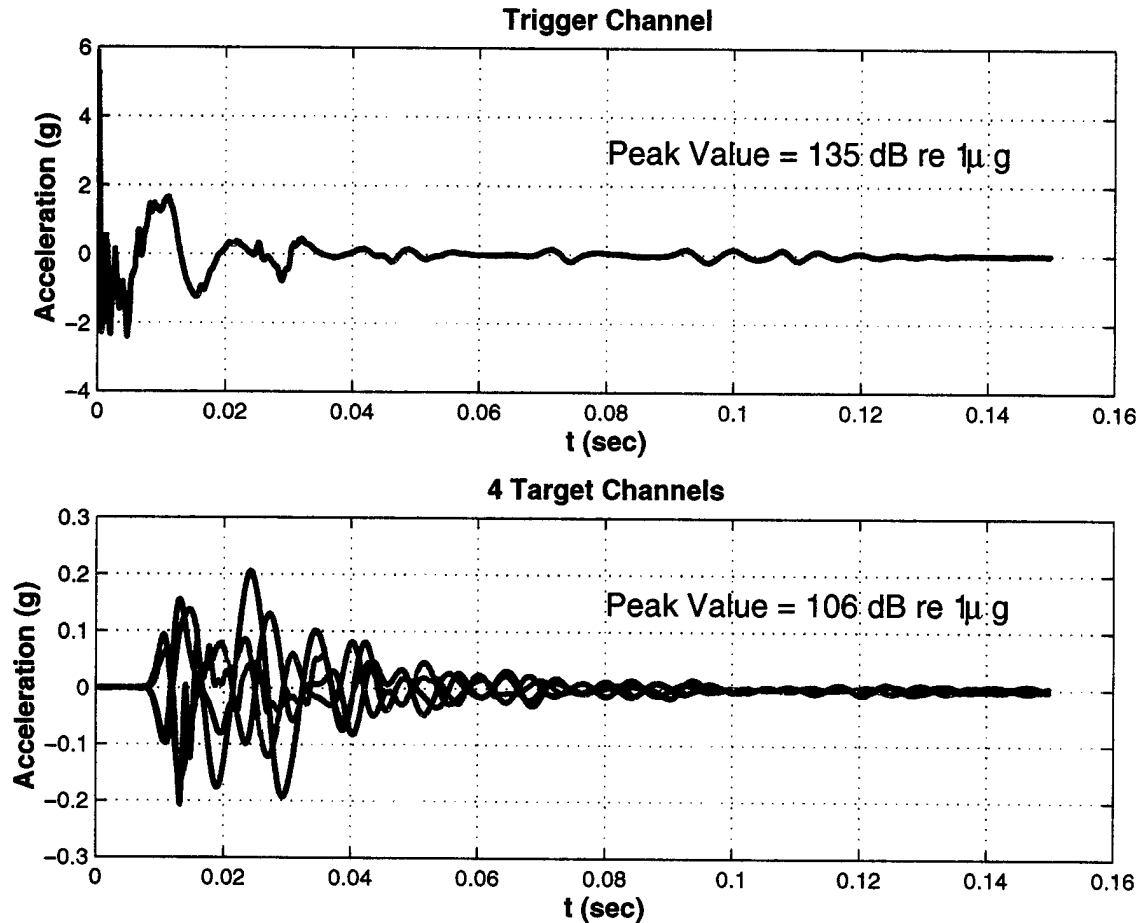
Figure 4-4. Measured Accelerations: The upper part of the figure shows the measured accelerations on a geophone at the surface of the earth at close proximity to the source and the lower part of the figure shows the accelerations measured by an accelerometer buried three feet down from the surface.

To compare these results with the output of the particle acceleration prediction programs it was necessary to measure the seismic velocities, V_p and V_s, to measure the attenuation, Q, to estimate the value of the density, ρ and to estimate the value of the source's force, F. The measured seismic velocities at the New Hampshire test site were measured to be V_p = 190 m/s and V_s = 110 m/s. The

measured attenuation was Q = 17. The density was estimated at ρ =1900 Kg/m^3 and from previous experiments with load cells the source was known to deliver approximately 8900 Newtons of force.

Using the above parameters the estimated particle accelerations are as shown in Figure 4-5. The source is located in the upper left-hand corner of the plot and the location of the buried accelerometers is indicated by a white dot. As can be seen from the color bar on the right side of the figure the estimated accelerations at both the source geophone and the buried accelerometers corresponds well to what was measured at the New Hampshire test site.
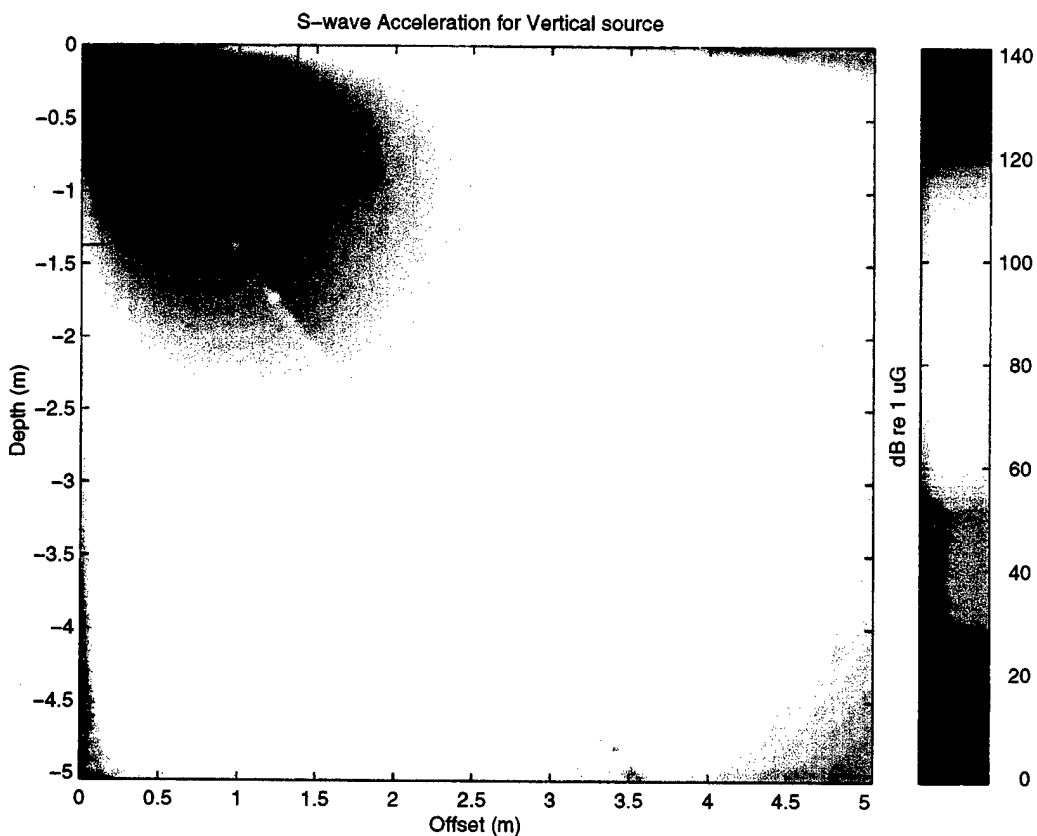
(F = 8909 N, f = 800 Hz, rho = 1900 Kg/m^3, Vp = 190 m/s, Vs = 110 m/s, M = 4.5 Kg, a = 0.0762 m, Q = 17)

Figure 4-5. Model Accelerations: The geometry of source and sensor locations corresponding to Figure 4-4 are shown; the color bar at the right shows the measured and modeled accelerations agree well..

4.2.5. Conclusions

With respect to detecting UXO with seismic waves the following conclusion may be drawn. The figures for shear waves indicate that for a shaker force of 10 pounds and a Q=50 the round trip attenuation to a target at 5 m offset and 2.5 m depth yields particle accelerations greatly in excess of 1 μg for a wavelength of 10 cm. This seems to indicate that after accounting for the target reflection strength and propagation effects back to the surface that recorded waves will continue to have accelerations in excess of 1 μg.

Commercially available accelerometers exist which have only a 1 μg noise floor over frequencies of interest to UXO detection. The conclusion is that under these circumstances no additional signal integration is necessary in order to achieve a sufficient SNR from the received signal.

Finally, the New Hampshire test site data validates the results of our prediction programs.

4.3. Simulating Synthetic Seismic Data

The second technical objective of the UXO project described in this section is the creation of synthetic data. The ability to create synthetic data is very important since it allows the testing of the design of data acquisition arrays as well as the performance of data processing algorithms. This section describes the methodology used to create synthetic data.

The methodology for creating synthetic data is based on several assumptions. The first is that the propagation affects obey the high frequency approximation to the elastic wave equation. This means that only travel time and geometric spreading need to be accounted for. Furthermore, it is presumed that the spectral content of the source is preserved at the receiver. Thus, if a source spectrum is presumed, all that is required to create a synthetic data set is to determine the

ensemble of all travel times from all sources to all receivers. This collection of travel times will include direct P and Rayleigh arrivals from a source to a receiver as well as reflections from a potential target. Furthermore, the synthetic data set will contain reflected arrivals for both the compressional and shear waves.

The primary problem in generating the synthetic data is in determining the exact location on the target which gives rise to a specular reflection between the source and the receiver. The specular reflection is just that which has the angle of incidence from the source equal to the angle of reflection to the receiver. Figure 4-6 illustrates the problem for a cylindrical target.

The program that was written to compute synthetic data for the UXO program was based on the assumption of a cylindrical target. The program determines the specular reflections points on a cylinder for all source receiver pairs in an acquisition geometry. Given these points the resulting travel times from source to receiver for a reflection off the target can be determined by computing the distance and dividing by the wave velocity. This velocity is different for shear and compressional waves, however, the specular reflection point does not change.
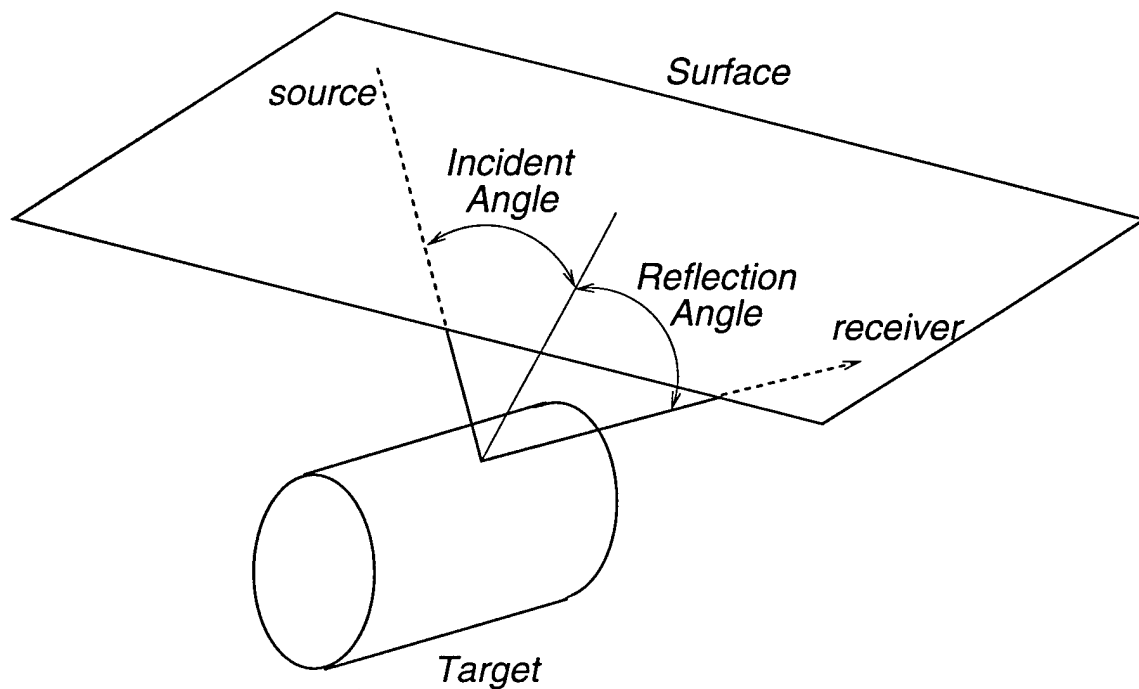
Figure 4-6. Specular Point on a Cylindrical Target: The source and receiver locations on the earth's surface give rise to a specular reflection (angle of incidence equals angle of reflection) on the cylindrical target. The collection of all specular points for all source receiver pairs must be found.

In order to determine the specular reflection point for all source receiver pairs it was necessary to solve the problem with a Newton search technique. The specular points satisfy three equations which are determined by making the angle of incidence equal to the angle of reflection and by specifying the radius of the cylinder. For S, P, and R the source, specular point, and receiver locations the roots of the following equations must be found.

$$\overline{SP} \cdot N - \overline{RP} \cdot N = 0 \qquad (1)$$
$$\overline{SP} \times \overline{RP} \cdot N = 0 \qquad (2)$$
$$P_y^2 + P_z^2 - r^2 = 0 \qquad (3)$$

where $\overline{XY}$ is the vector defined by the line between X and Y, x indicates the cross product, and is the dot product.

Figure 4-7 illustrates a test geometry used to 2D array data at a site in New Hampshire. The figure shows the receiver locations as circles, the source locations as stars, and the target location is the slender rectangle in the center of the plot. The sources and receivers are located at the surface of the earth and the target is at a depth of 3 feet.
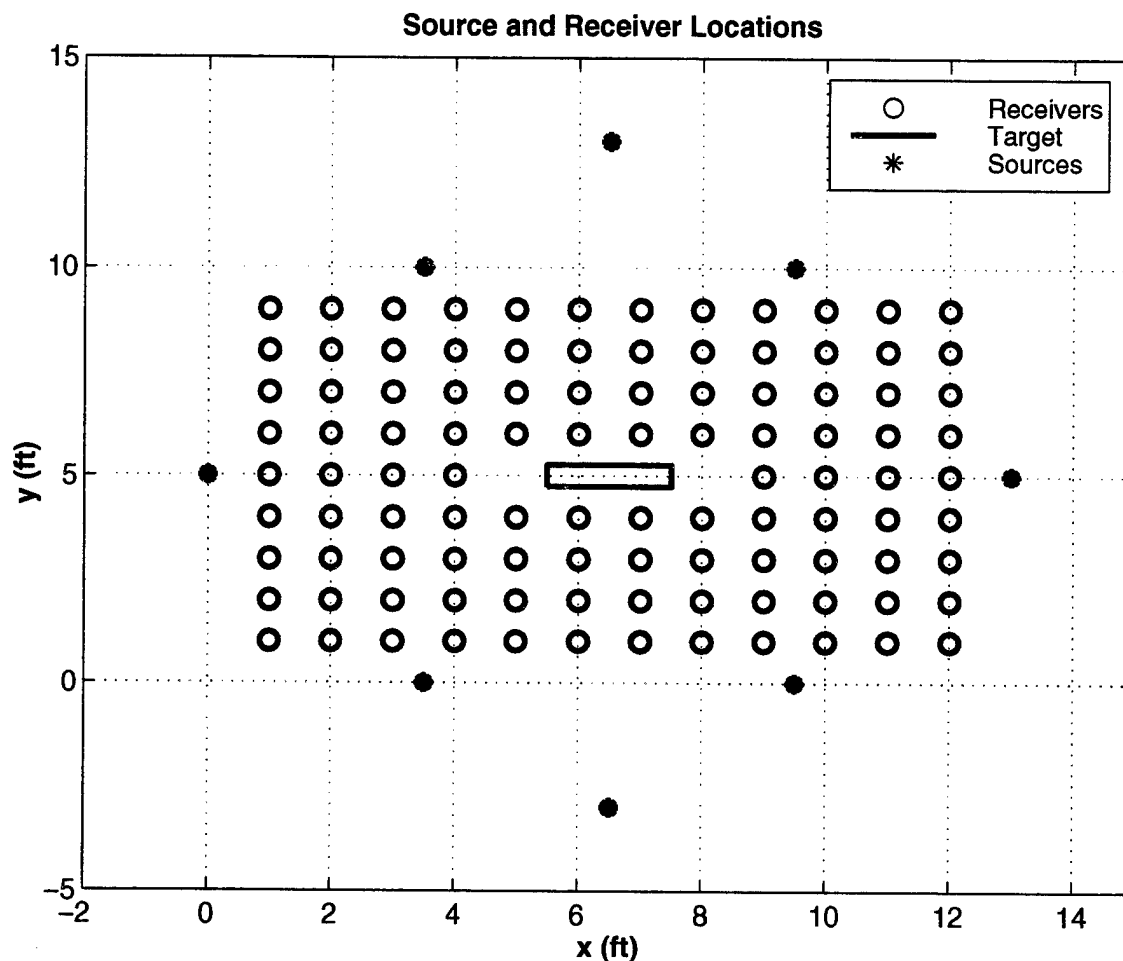

Figure 4-7, Acquisition Geometry: The circles represent receiver locations, the stars represent source locations, and the rectangle illustrates the positioning of the cylindrical target (at a depth of 3 ft.).

The associated synthetic data generated for testing the acquisition geometry are illustrated in Figure 4-7 is shown in Figure 4-8.

The usefulness of the synthetic data generator will be seen in the next section where the programs used for 3D imaging are described. The synthetic data permits the test of the 3D imaging algorithms and, in addition, allows for iterative design of the acquisition geometry. That is, various geometries can be postulated, used to generate synthetic data, and which is then imaged. If the result is acceptable then the acquisition geometry can be used in the field. If the result is unacceptable then the acquisition geometry must be redesigned.
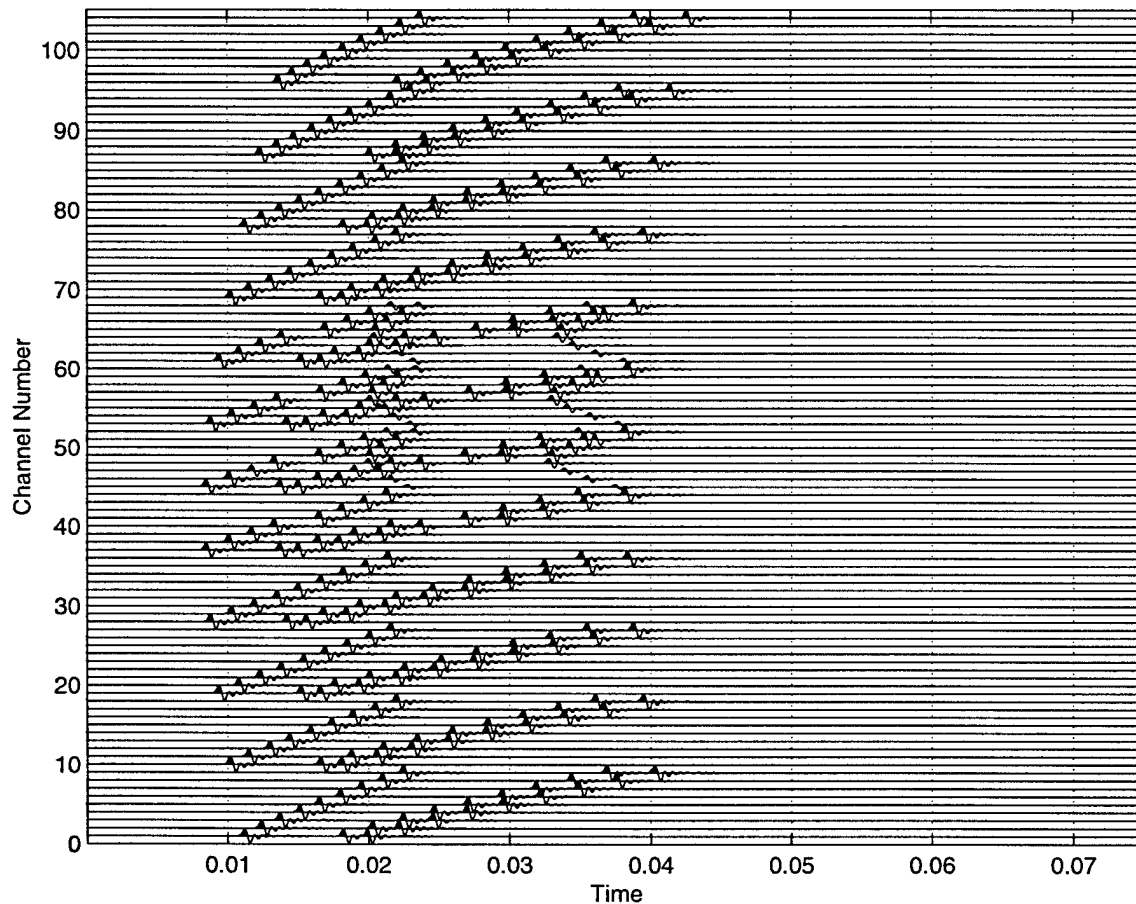

Figure 4-8. Synthetic Data Showing Direct Arrivals and Reflected Compressional and Shear Waves: The figure shows the amplitudes of the traces of each channel of the acquisition geometry as a function of time.

4.4. 3D Imaging of Seismic Data

The particle acceleration predictions analysis indicates that sufficient signal-to-noise ratio is obtained under most operating conditions for our seismic UXO detection scheme. Furthermore, the second section illustrates that using the acquisition geometry shown in Figure 4-7 yields synthetic data which has useful seismic reflections coming from the target (see Figure 4-8). This final section describes then how acquired data at the surface of the earth can be converted into a 3D image of the earth's interior and, thus, helping localize and identify potential targets.

Figure 4-9 conceptually explains how the 3D imaging of data is performed. The figure illustrates a source and a receiver positioned on the surface of the earth. As shown in the figure, the receiver records a reflection event in time. Given the wave velocity of the earth the reflection event's travel time can be used to determine the set of all possible points in the earth that could have caused the reflection. The collection of points, as shown in the figure, is just an ellipsoid.
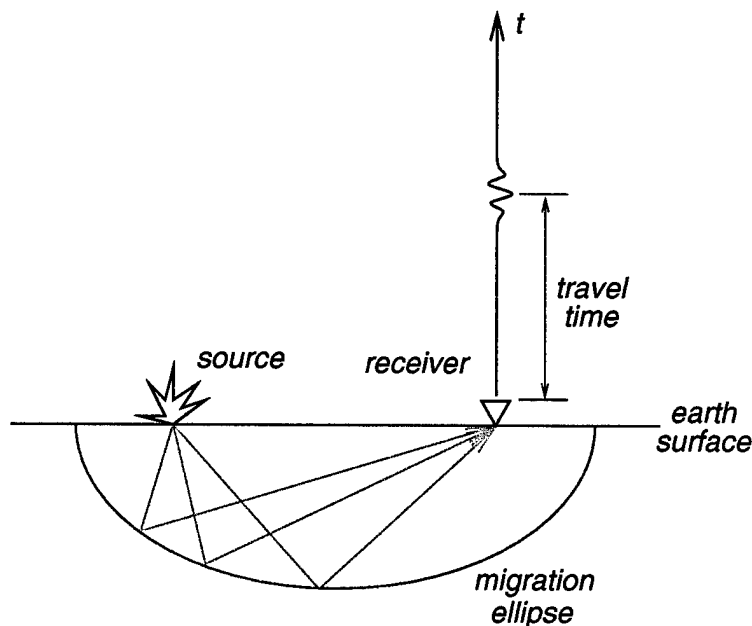

Figure 4-9. 3D Imaging Paradigm: Recorded reflection event could have been created by any point on an elliptic surface in the earth where the source and receiver locations form the ellipse foci. Thus, the surface data is imaged by smearing the reflection amplitudes along the elliptic surfaces.

The 3D imaging paradigm works by smearing the reflection amplitudes along ellipsoidal surfaces. The superposition of all reflection events from all source-receiver pairs creates the final 3D image. In the literature this procedure is known is Kirchhoff's integral. It has been shown that for sufficient source-receiver coverage of the earth's surface that the parts of the ellipsoidal surfaces which correspond to real reflectors are retained by constructive superposition of the recorded data and that the parts that do not are eliminated by destructive superposition.

To illustrate the method, the synthetic data shown in Figure 4-8 is 3D imaged and the results are shown in Figure 4-10, which shows slices through the 3D image cube. The slices are positioned so as to cut through the target cylinder. The presence of the target is clearly seen in the figure. Also visible, especially at the ends of the target, are wispy elliptical artifacts. This is due to the fact that insufficient source-receiver pairs cover this part of the image cube. The lower right graph in the figure shows a different display of the same 3D image cube. Here the display shows only those points of the cube which have amplitudes greater than a specified threshold. For this particular illustration the threshold was chosen to be 0.575 from a range of [0,1]. The position of the target is clearly visible in the figure. Furthermore, from the choice of threshold it can be seen that the target response is relatively strong in comparison to the background imaging artifact noise.
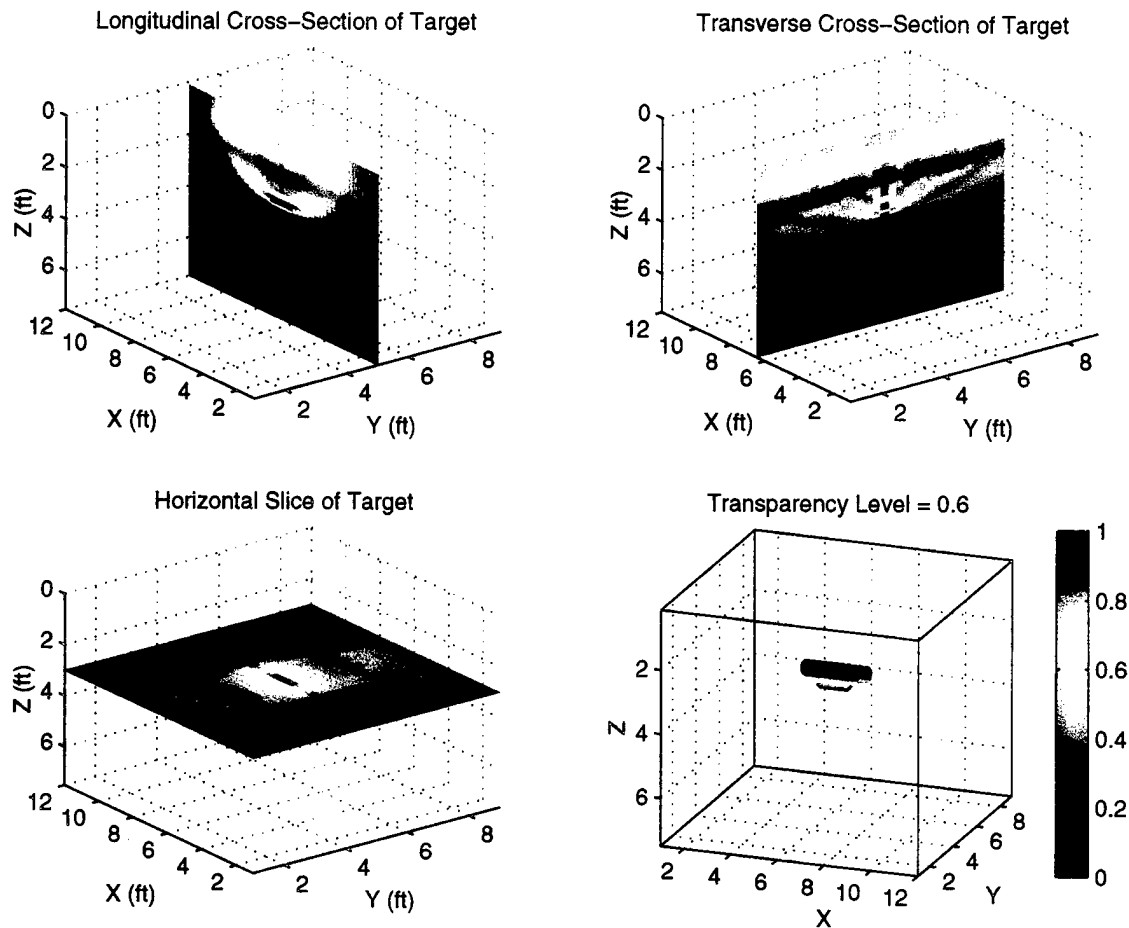
Figure 4-10. 3D Target Images from Synthetic Data: The target that is located at a depth of 3 ft. and positioned as illustrated by the acquisition geometry shown in Figure 4-7 is clearly seen in the slices from the 3D imaged data. Lower right graph shows the positions of points which exceed a threshold of 0.575 in a range of [0,1].

4.5. References

[4-1] Miller, G.F., and H. Pursey. "The field and radiation impedance of mechanical radiators on the free surface of a semi-infinite isotropic solid," *Proc. R. Soc. Lond.*, A223:521-41, 1954.

5. Conclusions and Future Analysis

5.1. Conclusions

The research so far has led to at least partial answers to key questions regarding the feasibility of Seismic Ordnance Detection.

What frequency seismic waves and what wavelengths propagate in the shallow earth? Significant seismic energy can be detected at a depth of 1 meter from vibrator sources strongly at 1000 Hz and up to 2000 Hz. At a shear wave velocity of 110 m/sec, this translates to wavelengths of 5 to 11 cm. This wavelength is short enough to detect UXO from mortar size up.

What is the practical bandwidth for a Seismic Ordnance Detection System? Consistent, coherent seismic energy up to at least 1500 Hz is practical. Seismic energy below 200 Hz is undesirable, since it is dominated by surface waves, which have long wavelength and do not penetrate into the ground. A band from 200 to 2000 is practical for seismic response analysis.

Can source coupling methods be improved to generate more high frequency seismic waves? Different coupling methods for sources result in increased high frequency coupling. In comparison with a flat horizontal disk, a source coupling method using a wedge that penetrates the soft surface and has large contact area shows improvements of 8–10 dB at frequencies above 500 Hz. Additional refinements can improve high frequency input and make desirable source directivity.

Is it practical to image shallow buried objects and to what resolution? Simulations of arrays with realistic seismic velocities and a seismic pulse of 100-800 Hz show that object shape and orientation can readily be imaged for a 2 foot long cylinder with appropriate 2D surface arrays.

Are there identifying characteristics in the response of ordnance to seismic waves that will allow discriminating UXO from clutter, and do they fall within the practical bandwidth? Both finite element modeling and in situ testing of a mortar shell show that there are modal lines in the 1200Hz – 2 kHz range. These

characteristic responses occur at frequencies that are within the bandwidth of current transducer systems.

What represents the noise limitation of the seismic system? This is currently under analysis as we develop a full system simulation. Work to this point indicates that reverberation caused by a seismic source dominates other noise sources when using a high force level source such as a hammer. When using a small vibrator, electronic noise and leakage from 60 Hz harmonics degrade proper processing of the sweep signal, resulting in noise contamination.

5.2. Ongoing and Future Work

- The most critical issue is the analysis of reverberation generated by the seismic source. This energy arrives at a receiver array in a random way and limits the detectability of target response at the surface. We are analyzing reverberation with both downhole three-component data and closely spaced 2D surface arrays.

- We are quantitatively analyzing the coherence of paths from sources to targets with measured downhole data to quantify potential array gain available by using many sources and receivers to overcome reverberation.

- We are assessing coupling consistency of seismic sources to the ground, to enhance high frequency output and to potentially reduce reverberation with source directivity.

- We are developing more complete system simulations to aid in development of a suitable array for Seismic Ordnance Detection. The key issues are what kinds of arrays are required for (1) noise suppression and for (2) imaging of objects.

- We will continue to address the question of what features of the seismic response will discriminate live UXO from false targets. As money allows we will do more modeling and complete verification of farfield response characteristics.

- When these questions are sufficiently analyzed we will derive a specification for a proof-of-concept system. Subsequent to this specification we will move on to advanced source, receiver and processing design.

APPENDIX A

Fourier Coefficients for Displacements and Stresses Due to Incident P, SV and SH Waves
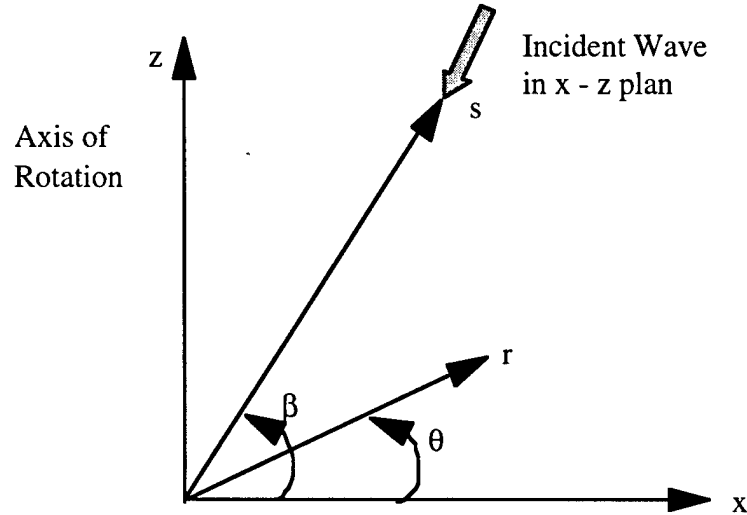
Displacements

	(P & SV)	(SH)
	$U_r = \sum_n U_{rn} \cos n\theta$	$\sin n\theta$
	$U_\theta = \sum_n U_{\theta n} \sin n\theta$	$\cos n\theta$
	$U_z = \sum_n U_{zn} \cos n\theta$	0

Stresses

	(P & SV)	(SH)
	$\sigma_r = \sum_n \sigma_{rn} \cos n\theta$	$\sin n\theta$
	$\sigma_\theta = \sum_n \sigma_{\theta n} \sin n\theta$	0

$$\sigma_z = \sum \sigma_{zn} \cos n\theta \qquad\qquad \text{sin } n\theta$$

$$\tau_{\theta z} = \sum \tau_{\theta z,n} \sin n\theta \qquad\qquad \text{cos } n\theta$$

$$\tau_{rz} = \sum \tau_{rz,n} \cos n\theta \qquad\qquad \text{sin } n\theta$$

$$\tau_{r\theta} = \sum \tau_{r\theta,n} \sin n\theta \quad \text{cos } n\theta$$

P – Wave (Δ_p = magnitude)

$$U_{rn} = A_n \cos \beta \, f_n'(\alpha)$$
$$U_{\theta n} = -n \, A_n \cos \beta \, f_n(\alpha)/\alpha$$
$$U_{zn} = i \, A_n \sin \beta \, f_n(\alpha)$$

where

$$c_1 = \left[(\lambda + 2\mu)/\rho\right]^{1/2} \qquad \lambda, \mu = \textit{Lame constants}$$

$$k_1 = \omega/c_1$$

$$A_n = -i \, \Delta_p \varepsilon_n \, exp(ik_1 z \sin \beta)/2\pi$$

$$\alpha = k_1 r \cos \beta$$

$$\varepsilon_n = \begin{cases} 1 & n = 0 \\ 2 & n > 0 \end{cases}$$

$$f_n(\alpha) = 2\pi(i)^n J_n(\alpha)$$

$$f_n'(\alpha) = \pi(i)^n \left[J_{n-1}(\alpha) - J_{n+1}(\alpha)\right]$$

$$f_n''(\alpha) = \pi(i)^n \left[(J_{n-2}(\alpha) + J_{n+2}(\alpha))/2 - J_n(\alpha)\right]$$

$$\sigma_{rn} = \sigma_{rn1} + \sigma_{rn2}$$
$$\sigma_{rn1} = -\lambda k_1 A_n f_n(\alpha)$$
$$\sigma_{rn2} = 2\mu k_1 A_n \cos^2 \beta f_n''(\alpha)$$

$$\sigma_{zn} = \sigma_{zn1} + \sigma_{zn2}$$

$$\sigma_{zn1} = \sigma_{rn1}$$

$$\sigma_{zn2} = -2\mu k_1 A_n \sin^2 \beta f_n(\alpha)$$

$$\sigma_{\theta n} = -A_n \left(\lambda k_1^2 + 2\mu n^2 / r^2\right) f_n(\alpha) / k_1 + 2\mu A_n \cos \beta f_n'(\alpha) / r$$

$$\tau_{\theta z,n} = -i2\mu n \sin \beta A_n f_n(\alpha) / r$$

$$\tau_{rz,n} = -i2\mu k_1 \cos \beta \sin \beta A_n f_n'(\alpha)$$

$$\tau_{r\theta,n} = 2\mu n A_n \left[f_n(\alpha) - \alpha f_n'(\alpha)\right] / \left(k_1 r^2\right)$$

SV – Wave (Δ_{SV} = *magnitude*)

$$U_{rn} = ik_2 \sin \beta \cos \beta A_n f_n'(\alpha)$$

$$U_{\theta n} = -in \sin \beta A_n f_n(\alpha) / r$$

$$U_{zn} = A_n \left[n^2 f_n(\alpha) / \left(k_2 r^2\right) - \cos \beta f_n'(\alpha) / r - k_2 \cos^2 \beta f_n''(\alpha)\right]$$

where

$$c_2 = (\mu / \rho)^{1/2}$$

$$k_2 = \omega / c_2$$

$$\alpha = k_2 r \cos \beta$$

$$A_n = \Delta_{SV} \varepsilon_n \, exp(ik_2 z \sin \beta) / \left(2\pi k_2 \cos \beta\right)$$

$$\varepsilon_n, f_n, f_n' \; and \; f_n'' \; same \; as \; for \; P\text{-}wave$$

$$\sigma_{rn} = 2ik_2^2 \mu \sin \beta \cos^2 \beta A_n f_n''(\alpha)$$

$$\sigma_{\theta n} = 2i\mu A_n \left[k_2 \sin \beta \cos \beta f_n'(\alpha) - n^2 \sin \beta f_n(\alpha) / r\right]$$

$$\sigma_{zn} = 2ik_2^2 \mu \sin \beta \cos^2 \beta A_n f_n(\alpha)$$

$$\tau_{\theta z,n} = -n\mu k_2 \cos^2 \beta A_n f_n(\alpha) / r$$

$$\tau_{rz,n} = -\mu k_2^2 \cos \beta \cos 2\beta A_n f_n'(\alpha)$$

$$\tau_{r\theta,n} = 2i\mu n \sin \beta A_n \left[f_n(\alpha) / r - k_2 \cos \beta f_n'(\alpha)\right] / r$$

SH – Wave (Δ_{SH} = magnitude)

$U_{rn} = -n A_n / r$

$U_{\theta n} = -k_2 \cos \beta A_n f_n'(\alpha)$

where

$$A_n = i \Delta_{SH} \varepsilon_n \exp(i k_2 z \sin \beta) / (2 \pi k_2 \cos \beta)$$

all other definitions same as for SV - wave

$\sigma_{rn} = 2 \mu n A_n \left[f_n(\alpha) / r - k_2 \cos \beta f_n'(\alpha) \right] / r$

$\sigma_{\theta n} = 2 \mu n A_n \left[-f_n(\alpha) / r + k_2 \cos \beta f_n'(\alpha) \right] / r$

$\tau_{\theta z, n} = -i \mu k_2^2 \cos \beta \sin \beta A_n f_n'(\alpha)$

$\tau_{rz, n} = -i n \mu k_2 \sin \beta A_n f_n(\alpha)$

$\tau_{r\theta, n} = \mu A_n \left[k_2 \cos \beta f_n'(\alpha) / r - n^2 f_n(\alpha) / r^2 - (k_2 \cos \beta)^2 f_n''(\alpha) \right]$

APPENDIX B

Seismic Sonar for Landmine and UXO Detection and Classification

Paper presented at the Third International Symposium on Technology and the Mine Problem,
Monterey, Calif., April 1998

Peter A. Krumhansl

GTE - BBN Technologies
70 Fawcett Street
Cambridge, MA 02138
617-873-4158
617-547-8918 (fax)
pak@bbn.com

Seismic Sonar for Landmine and UXO Detection and Classification

Peter A. Krumhansl

Introduction

Current buried ordnance sensing technologies have evolved over a long period of time and can be very effective within their sensing and environmental limitations. Magnetometers, electromagnetic sensors (EM), and ground penetrating radar (GPR) primarily detect the ferrous content or electrical conductivity properties of buried materials. Detection rates for these sensors can be high, but the false target rate can run as high as 4:1 or higher. Detection of nonmetallic objects is difficult.

Seismic technologies have proven highly successful in oil exploration, geotechnical, and environmental work. They provide a means of remote sensing the **mechanical properties** of materials or objects below the surface of the ground. A seismic sensor can detect nonmetallic landmines or ordnance and can provide a different "look" at a buried object to better classify them. Seismic systems can also operate in environmental conditions which adversely affect other sensors.

BBN is currently developing a seismic sonar system for detecting unexploded ordnance (UXO) that is buried up to 5 meters below the surface. We have previously developed and field tested an experimental system that detects buried landmines with seismic surface waves. This technology locates anti-tank mines buried up to a foot deep from a safe, standoff position. The system detects mines in a 6 by 6 meter search area adjacent to the foot print of the system. This seismic technology is currently being extended to search for UXO, hazardous waste, and other objects buried at depths up to 5 meters or more.

Standard seismic techniques and equipment used in geotechnical engineering applications or scaled-down versions of seismic methods used in oil exploration are not suitable for detecting buried UXO. They are either designed to find layered geology or have field techniques that are extremely expensive to cover a 3-D volume. BBN has developed an approach that is more similar to an active sonar system. An array of seismic sources propagates seismic waves into the search area, and an array of receivers picks up echoes from objects (Figure 1).
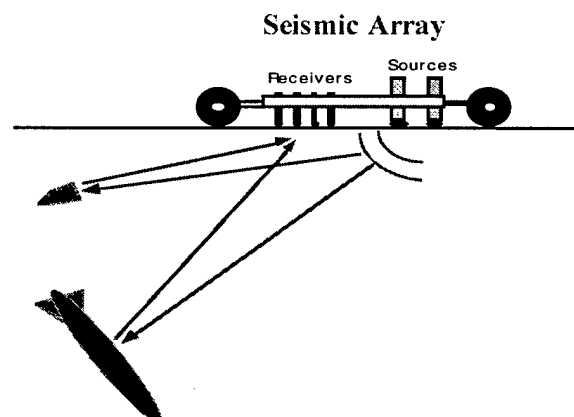

Figure 1. Seismic sonar system concept

The use of a 2-D array of seismic receivers and controllable sources allows focusing of the necessary short wavelength seismic energy both downward and outward from the array on the surface. A point focused, nearfield beamformer is then used to suppress reverberation and to detect and locate small objects close to the array. This approach is called seismic sonar.

First, a brief discussion of seismic wave propagation is presented as it relates to detecting different objects in the subsurface. This is followed by a summary of the successful development of the seismic landmine detection technology. Finally, initial experiments and system development for UXO detection are described.

Seismic Waves for Subsurface Detection

A seismic source that applies a vertical point force on the surface of the soil produces a variety of propagating seismic wave types. Unlike acoustic media, which cannot transmit shear stress, an elastic medium such as soil propagates both compressional P waves and shear S waves. These waves travel through the volume of the subsurface and have particle motion that is polarized longitudinally and transverse to the direction of propagation, respectively (Figure 2). Additionally, from a surface seismic source, Rayleigh waves propagate along the boundary with an elliptical particle motion polarization. The particle motion of Rayleigh waves dies off rapidly with depth, extending

down only about a wavelength. Any of these wave types can be used as the basis for a subsurface detection system, depending on the goal of the survey.
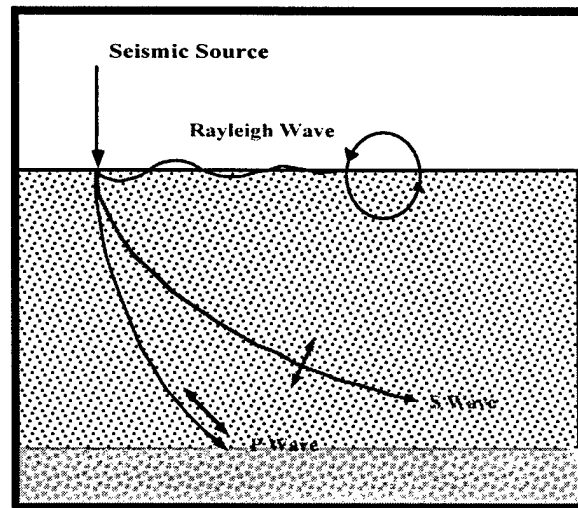

Figure 2. Waves in Soils for a Vertical Point Force

The three wave types have different velocities, depending on the bulk and shear modulus of the soils and their density. The P wave is fastest, with typical speeds of 240-340 m/sec in the top 2-3m of unconsolidated soils. Rayleigh waves are slowest, with measured speeds of 100-200 m/sec at frequencies of 75-300 Hz. The S waves near the surface travel at speeds typically 10% faster than the Rayleigh wave. The relevance of these different wave speeds is that for a given source frequency, P waves have the longest wavelength, approximately twice that of Rayleigh and shear waves. This wavelength determines both the resolution of the system and the strength of the echo from an object.

The seismic properties and hence the P and S wave speeds, vary with depth. This is due to the compaction of the soil under the weight of the overlying material, which causes refraction of the P and S waves and dispersion of the Rayleigh wave. Interrogation of the subsurface below a depth of 1 to 2m must take the velocity variation into account to precisely locate and accurately beamform the echo.

Use of Rayleigh wave for detecting very shallow objects. For detecting very shallow objects such as landmines or very shallow buried ordnance, the Rayleigh wave has several advantages. It is by nature confined to a layer near the surface of the earth and thus illuminates only the region where the targets are located. An associated characteristic is that geometrical spreading for a surface wave is cylindrical rather than spherical, resulting in less signal loss with distance. This improves system signal to noise and range of detection. The Rayleigh wave has the shortest wavelength and is thus capable of resolving smaller objects. Another advantage is that Rayleigh wave echoes arrive later than direct and refracted energy. This means that the noise of these strong wave types does not interfere with weak reflected echoes from landmines. The BBN seismic landmine detection system successfully uses Rayleigh waves to detect shallow buried mines.

Seismic wave types for deeper targets. For detecting deeper objects, either the P wave or the S wave must be used. Both are commonly used for seismic reflection profiling for oil or geotechnical studies. Figure 3 shows the radiation directivity pattern of the P and vertically polarized Sv shear waves for a vertical point force on the surface. These were computed for a half space with constant seismic properties. The P wave has a simple directivity pattern with a downward pointing maximum and a horizontal null. The Sv wave has one null straight down and a second at 30°, but has higher levels than the P wave over most angles and remains strong up to shallow angles. A tilted source can also produce horizontally polarized Sh shear waves, which propagate straight down. P, Sv, and Sh waves each have advantages and disadvantages for UXO detection.

Targets of seismic detection systems. Seismic detection systems investigate the subsurface for objects with anomalous mechanical properties. The seismic waves propagate through the soil at a velocity related to the mechanical stiffness and density of the compacted matrix of soil particles. When a zone of materials with different properties is encountered, some of the seismic energy is reflected. Objects such as landmines, bombs, or projectiles with solid casings are much stiffer and more dense than typical soils. These objects tend to move as rigid bodies surrounded by the spring of the unconsolidated soil. Both translational motion and rocking motion of the body

occurs depending on the incident seismic wave and the objects orientation. Additionally, an objects mechanical resonances can be excited by the seismic wave. The object's response when excited by an incident seismic wave effectively scatters energy that can be detected as an echo at remote vibration receivers.
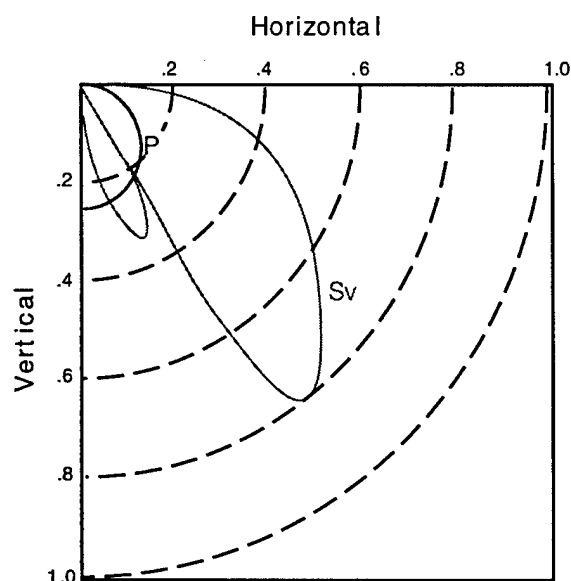

Figure 3. Directivity Plots of P and S waves for Vertical Source on Halfspace (σ = 1/3)

Seismic Landmine Detection Technology

BBN was funded by the US Army from 1988-1993 to investigate the feasibility of detecting landmines with acoustic or seismic methods. This program resulted in an extensive development effort that spanned a broad range of research, including seismic properties of very shallow soils, transducer development for high frequency seismic applications, new algorithms for beamforming or imaging, and data acquisition system development. The result was the successful demonstration of an experimental seismic mine detection system in a number of soils in Massachusetts.

The primary objective of this study was to detect antitank mines, which range from 8 to 12 inches across and are from 3 to 4 inches thick, buried in the top 12 inches of soil. A typical target is a Russian TM-46 mine. Detecting smaller anti-personnel mines was a secondary objective.

From the start, tests were performed in natural soils rather than in artificial lab environments to facilitate realistic system development. This approach provided early measurement of soil characteristics and mine echoes, allowed us to become familiar with naturally occurring clutter, and in the future will make the transition to a fieldable system more direct. Successful tests were performed in a variety of sandy soils developed on glacial deposits in Massachusetts. These tests spanned a range of conditions with different amounts of rocks, vegetation, and moisture.

Seismic mine detection system concept. Results of our preliminary investigation of acoustic techniques indicated that coupling acoustic energy across the air/ground interface was difficult due to the high impedance contrast between the soil and the air. Ground contacting seismic sources are much more efficient at generating a propagating wave in the ground that can be used to detect a subsurface target. A system

concept was developed for a mobile system with ground contacting seismic sources and receivers (Figure 1).

The basic operation of the seismic landmine detection system is similar to an active sonar system adapted to soils. A broadband, impulsive Rayleigh surface wave is generated by an array of seismic sources. The Rayleigh waves propagate along the surface of the ground out into the search area in front of the system. If a buried mine is encountered, a portion of the energy is reflected back due to the contrast in the mechanical properties between the mine and the soil. The reflected signals are received by a two-dimensional array of geophones that individually sense the vertical ground motion. These signals are digitally recorded, bandpass filtered, and beamformed. The amplitude and location of the scattered energy is then displayed in an x-y map of the search area. Due to increased transmission loss at high frequencies, mines are typically detected with wavelengths longer than their size, resulting in echoes that are a composite response of the whole target. The echo's amplitude, phase, frequency content, and shape are used to distinguish mines from rocks, holes, or other geologic features.

Seismic Transducers. Commercial seismic sources and receivers did not meet the requirements for seismic mine detection. As a result, we examined the physics of soils and transducer coupling for high-frequency Rayleigh wave generation and ground motion coupling. We engineered and tested a variety of seismic sources including sparkers, weight drops, small gun blanks, and vibrators. An improved geophone design which compressed the soil under the transducer resulted in significantly broader bandwidth.

For landmine detection the seismic source is required to generate Rayleigh waves over the band from 50-500 Hz. The sources must be highly repeatable from shot to shot and position to position, because in the beamforming process, signals from different sources are combined. Because the temporal duration of the wavelet defines the range resolution of the system, a clean seismic pulse with minimal ringdown is important. For mounting on a mobile array, a compact source is desirable.

For experimental purposes, we developed a land sparker source similar to a marine sparker. An electrode is placed at the bottom of a tube filled with salt water. An EG&G 300-joule power source dumps its energy to the electrode, producing a spark. The shock wave is transmitted through a flexible diaphragm into the ground. The column of water and sheets of thin foam rubber in the upper part of the water column confine the bubble and absorb the acoustic energy moving up the tube. Measurements with a force gauge showed that the source generated about 2000 lbs peak force and had significant energy to over 800 Hz.

We performed numerous successful detection experiments with the sparker source described above, but eventually found it to be a limiting factor in the landmine detection system. The sparker and other impulsive sources are limited in the amount of high frequency energy coupling to the Rayleigh wave by the physics of the impact on the soil. Under the high impact forces generated by these sources, the soil deforms and less high frequency energy is coupled into the soil, particularly into the Rayleigh wave. Also, the sparker and the weight drop sources had significant ringdown, which resulted in noise in the detection display and high false alarm rates. Efforts at deconvolution were unsuccessful due to the presence of both P and Rayleigh waves with different spectral characteristics.

Due to these limitations, we adapted and tested a compact moving armature seismic vibrator developed by BBN for Navy applications. This vibrator was capable of 100 lbs force output over the band 50 to 200 Hz and useful levels up to 400 Hz and has harmonic distortion of less than -35 dB. Using a linear sweep from 50–400 Hz and correlating the result, source ringdown was reduced and clean Rayleigh waves were generated. A shaped spectrum correlation process was developed for the vibrator data which compensates for the coupling characteristics of the vibrator to the ground and compresses the output time waveform to minimize ringing in the time domain and improve resolution. High-frequency Rayleigh waves were generated in moist sand with the vibrator where the high peak force impulsive sources failed.

Seismic mine detection array. An experimental array consisting of four sources and 32 geophones was designed to transmit and receive the seismic signals. During data acquisition, each source transmits separately and each geophone's output is recorded separately, resulting in a total of 128 time records of seismic data. The array is spread over a two-dimensional area on the surface measuring 1.9 by 3.8 meters. The size and number of elements in the array were designed to provide the necessary resolution and to suppress reverberation and noise. The reverberation consists of unwanted reflected energy from subsurface layers and surface and volume heterogeneities. During all tests, the system's detection range and signal-to-noise ratio were limited by reverberation rather than ambient noise.

Data acquisition system. For data acquisition, BBN developed a flexible system based on the VME bus that allows for 64 channels of data acquisition at 8 kHz per channel. A controllable front end filter/preamp provides necessary signal conditioning prior to digitizing. A SUN SPARCstation or PC is used in the field for acquisition control, processing, and display.

Processing and nearfield beamforming. After the seismic data is acquired, it is processed to

give an image of the earth's reflectivity to Rayleigh waves over the search area. First, the time series is filtered with a bandpass filter centered at 200 Hz and two octaves wide. This removes noise and the long wavelength Rayleigh wave components. Then, the direct P and Rayleigh waves are muted out, leaving only the scattered signals in the time trace.

The data is then nearfield beamformed using a time delay beamformer. This beamformer sequentially scans every image point or pixel in the search area, which are typically spaced 0.1m apart. For each image point and source receiver pair, the algorithm computes the exact travel time for a Rayleigh wave to travel from the source position to the image point to the receiver and adds it to a source delay term. This source delay is the effective rise time of the Rayleigh wave as it develops and propagates away from the nearfield of the source. The amplitude of the received ground vibration at this total travel time is summed or stacked for that image point. This procedure is repeated for all source/receiver time records until all 128 traces have been summed for that image point. This process effectively focuses the array on the Rayleigh wave energy that has been scattered from this point in the search area. The entire process is repeated for all the image points until a 2-D image of the returned Rayleigh energy from the search area is developed. A scale factor is computed that compensates for attenuation and cylindrical spreading. This factor is applied so that amplitude of the displayed image is proportional to the strength of the scattered energy from that position in the ground. The amplitude of the scaled sum is then thresholded and displayed in an x-y map with red for positive values of returning signal and green for negative values.

Field procedures. In a our mine detection experiments, a radial line array was laid out and data taken to calibrate the seismic propagation velocities and transmission loss for the area. Then the 2-D landmine detection array was laid out and the seismic data acquired to measure the earth's natural reflectivity characteristics before any mine targets were buried. Holes were dug and a number of mines were buried, most often a TM-46 and a plastic M80 refilled with epoxy having the same density as explosives. The seismic data was acquired again, beamformed, and the result compared with the earth's background. An example of the detection output for high signal to noise is shown in Figure 4.
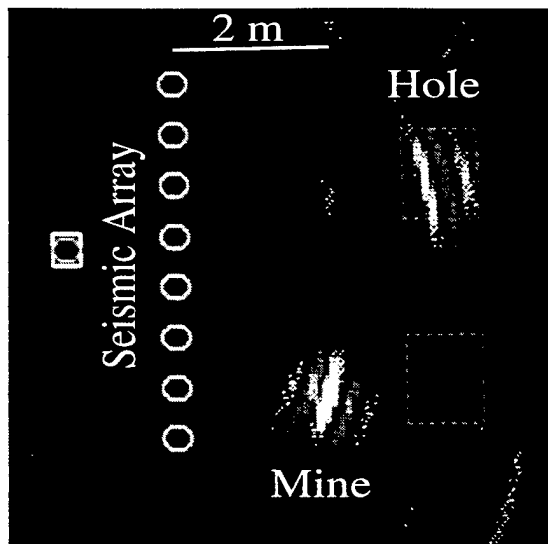
Figure 4. Seismic Landmine Detection at Sudbury Annex, Fort Devens, MA. Sandy Soil with Sparse Vegetation, AT Mine and 14" Hole

These results are from the Sudbury annex of Fort Devens, Mass., in a lightly vegetated field with a hard, compact surface. The display shows the seismic system response for a landmine buried at a range of 5 feet and a mine-size hole at a range of 10 feet. The mine and the hole are distinguishable by the difference in phase when displayed in color.

Overall, the seismic mine detection system was tested in 22 experiments in different soil types, including sandy soils with little vegetation and some rocks, loamy soils with moderate vegetation, a highly vegetated upland soil in a tilled field, and hard-packed dirt roads. These areas were tested under both dry summer conditions and wet conditions, including surface slush in late fall. The system did not work in the upland soil due to a highly dispersive guided wave in a low velocity surface layer. The system was

able to detect 12-inch diameter landmines in 75% of the trials at the other four sites at ranges up to 17 ft. Smaller 5-inch can-style anti-personnel mines were detected under optimal conditions. Mines were located with a precision of better than a meter and under good conditions, to a precision of 0.15m. False alarm rates varied from site to site, from near zero, even in the presence of rocks, to rates of 50%. Not enough samples are available for full characterization of Pfa and Pd in a range of soils. In all tests the seismic echo characteristics from mines were distinguishable in level or character from mine-size rocks and holes.

Summary of seismic landmine detection work
The feasibility of detecting metallic and non-metallic landmines with seismic waves was demonstrated. Analysis of system components indicates that modifications can be made to improve the detection and false alarm performance and precision of location. Analysis of results indicates that source ringdown and array design were responsible for a significant portion of false alarms for these data sets. Work is continuing on key technologies to improve performance.

UXO Detection System Development and Experiments

Work is beginning to adapt the seismic sonar concept to detecting unexploded ordnance at depths up to 5 meters. The seismic sonar system concept for detecting deeper buried objects is similar to the seismic landmine

detection system, with some modifications to hardware and software. The UXO detection system will search the volume below and to the sides of the array for each array location . The size of this volume will depend on the transmission loss of the seismic energy and the velocity profile. As the array is moved over the survey location, adjacent volumes will be processed coherently, searching a continuous volume of the earth for buried targets. This field procedure will also provide views of targets from different angles, which will provide information about orientation.

To compensate for the higher wave speeds of P and S waves, the seismic sonar system's bandwidth is being extended to 1200 Hz by improved designs of sources and geophones. The response of this improved geophone on sandy soil is shown in Figure 10 and is smooth and fairly flat to 1200 Hz. This is the response of the geophone coupled to the ground which is being shaken by a nearby calibration vibrator. Additionally, a new compact shaker is being tested with force output of over 50 lbs from 100 to 2000 Hz. This shaker is a variant of a moving armature design which has high output, low distortion (less than 1%), and proven reliability in a variety of conditions. Its compact size, about a 4-inch cube, allows small and light components to couple the force to the ground, which allows operation up to higher frequencies before structural modes develop in the body of the source. Additional

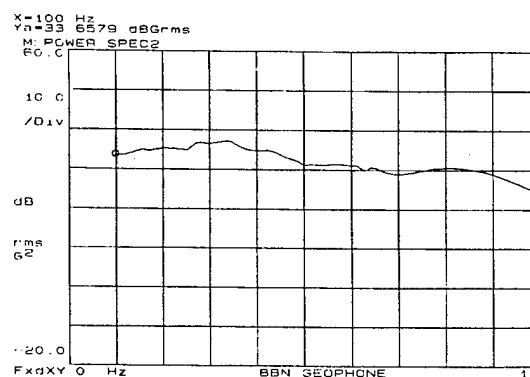engineering is being done to design the case and foot for coupling to the ground.

Figure 10. Modified geophone response showing sensitivity to 1200 Hz.

Diagnostic field tests to quantify seismic coupling, noise and transmission loss will begin in the summer of 1998 and will be used in systems analysis and redesign of the transducer arrays for detecting buried ordnance. The beamformer will be modified to search a volume with a depth varying velocity. A full elastic Finite Element Modeling capability is being developed for analyzing target strength of buried ordnance. This will lead to an analysis of detectability of buried bombs and a characterization of their seismic signatures. We will develop and build a proof of concept prototype for the Seismic Ordnance Detection System (SODS).

Summary

A seismic sonar system has been developed and successfully tested to locate shallow buried landmines. The system is being further developed to detect objects buried down to a depth of 5 meters. Initial field

measurements of transmission loss indicate the feasibility of using seismic shear waves to detect objects with diameters of 0.16m at depths of 2.4m. Larger objects may be detected at deeper levels. Seismic sources and receivers capable of coupling the required bandwidth seismic signal to the ground have been developed. Further system design of arrays and software is underway and field tests will begin this summer.

The development of a seismic sensor will result in a significant broadening of detection and classification capabilities, including the ability to detect non-metallic landmines, to operate in environments which limit other sensors, and to provide a sensor of the mechanical properties of detected targets to allow better classification. Significant savings will be achieved by incorporation of a practical seismic sensor into an appropriately structured ordnance site characterization and cleanup process.